

# Causes of the Regional Variability in Observed Sea Level, Sea Surface Temperature and Ocean Colour Over the Period 1993–2011

B. Meyssignac<sup>1</sup>  · C. G. Piecuch<sup>2</sup> · C. J. Merchant<sup>3</sup> ·  
M.-F. Racault<sup>4,5</sup> · H. Palanisamy<sup>1</sup> · C. MacIntosh<sup>3</sup> ·  
S. Sathyendranath<sup>4,5</sup> · R. Brewin<sup>4,5</sup>

Received: 22 March 2016 / Accepted: 11 August 2016  
© Springer Science+Business Media Dordrecht 2016

**Abstract** We analyse the regional variability in observed sea surface height (SSH), sea surface temperature (SST) and ocean colour (OC) from the ESA Climate Change Initiative datasets over the period 1993–2011. The analysis focuses on the signature of the ocean large-scale climate fluctuations driven by the atmospheric forcing and do not address the mesoscale variability. We use the ECCO version 4 ocean reanalysis to unravel the role of ocean transport and surface buoyancy fluxes in the observed SSH, SST and OC variability. We show that the SSH regional variability is dominated by the steric effect (except at high latitude) and is mainly shaped by ocean heat transport divergences with some contributions from the surface heat fluxes forcing that can be significant regionally (confirming earlier results). This is in contrast with the SST regional variability, which is the result of the compensation of surface heat fluxes by ocean heat transport in the mixed layer and arises from small departures around this background balance. Bringing together the results of SSH and SST analyses, we show that SSH and SST bear some common variability. This is because both SSH and SST variability show significant contributions from the surface heat fluxes forcing. It is evidenced by the high correlation between SST and buoyancy-forced SSH almost everywhere in the ocean except at high latitude. OC, which is determined by phytoplankton biomass, is governed by the availability of light and nutrients that essentially depend on climate fluctuations. For this reason, OC shows significant correlation with

---

**Electronic supplementary material** The online version of this article (doi:[10.1007/s10712-016-9383-1](https://doi.org/10.1007/s10712-016-9383-1)) contains supplementary material, which is available to authorized users.

---

✉ B. Meyssignac  
benoit.meyssignac@legos.obs-mip.fr

<sup>1</sup> LEGOS, CNES, CNRS, IRD, UPS, Université de Toulouse, 31000 Toulouse, France

<sup>2</sup> Atmospheric and Environmental Research, Inc., 131 Hartwell Avenue, Lexington, MA 02421, USA

<sup>3</sup> University of Reading, Reading RG6 6AH, UK

<sup>4</sup> Plymouth Marine Laboratory (PML), Prospect Place, The Hoe, Plymouth PL1 3DH, UK

<sup>5</sup> National Centre for Earth Observation (NCEO), PML, Plymouth PL1 3DH, UK

SST and SSH. We show that the correlation with SST displays the same pattern as the correlation with SSH with a negative correlation in the tropics and subtropics and a positive correlation at high latitude. We discuss the reasons for this pattern.

**Keywords** Sea level · Sea surface temperature · Ocean colour · Ocean heat content · Climate · ESA Climate Change Initiative · Wind forcing · Buoyancy forcing · ECCO reanalysis

## 1 Introduction

Oceans have been routinely monitored from space for more than 30 years now. In 1978, NASA launched Seasat, TIROS-N and Nimbus-7, the first three satellites dedicated to ocean observations. Seasat carried five complementary sensors and provided the first estimates from space of sea surface height (SSH), surface wind stress, sea surface temperature (SST), surface wave field and polar ice extent. Unfortunately, these estimates covered only a short period because Seasat failed after 105 days in space. TIROS-N lasted more than 2 years in orbit and produced the first really useful maps of SST. The Nimbus-7 carried the Coastal Zone Colour Scanner (CZCS), which remained operational for seven and a half years, from October 1978 until June 1986. CZCS was the first satellite sensor specifically developed to study ocean colour properties. Since then, about a dozen ocean-observing satellite missions have been launched by several space agencies to monitor continuously more than 10 essential ocean variables including SSH, ocean currents, tides, wave height (with radar altimeters), wind speed and direction (with microwave scatterometers), SST (with infrared and microwave radiometers), sea surface salinity (with microwave imaging radiometers with aperture synthesis), ocean colour (with multispectral imagers) and ocean bottom pressure (with space gravimetry).

In >30 years of measurements, satellite missions have revolutionized our understanding of the oceans. By providing a global mapping repeated with high temporal resolution, they have revealed the intense spatio-temporal variability, which characterizes the cycles of the oceans. This new picture challenged earlier views based on previous sparse measurements collected from ships and buoys. It spurred oceanographers to make considerable progress in the understanding of the role of the ocean in the physical (e.g., climate and weather), chemical (e.g., carbon cycle) and biological (e.g., primary production) processes of the Earth.

In this paper, we are interested in the role played by the ocean in the climate system. We revisit the 30-year-long satellite record of ocean observations and summarize what we have learned from it about the ocean variability at climatic timescales (i.e. interannual to multidecadal timescales). We take advantage of the satellite archive, which gives an almost global view of the oceans, to explore the regional ocean variability.

Among all ocean variables remotely sensed from space, SSH, SST and ocean colour (OC) have long enough continuous records ( $\sim 20$  years or longer) to address the inter-annual to multidecadal variability in the ocean. For this reason, we focus on these three variables. We also analyse the hydrographic data (temperature and salinity) obtained from in situ measurements because these data are covering a large part of the ocean since the 1970s (Rhein et al. 2013; Abraham et al. 2013) and provide highly valuable information to interpret the signal showed by the other variables. Our objectives are to (1) describe the

dominant spatio-temporal patterns of nonseasonal SSH, SST and OC variability, (2) discuss the current state of knowledge regarding the physical mechanisms responsible for these patterns and (3) explain the covariance at climatic timescales between these spatio-temporal patterns. The outline of the paper is as follows: Sect. 2 recalls the physical background governing the SSH, SST and OC variability and explains how this variability is linked to the atmospheric forcing and the ocean circulation. Section 3 shows the spatio-temporal patterns of SSH, SST and OC obtained from the satellite archive and uses the outputs of an ocean reanalysis to unravel the role of the atmospheric forcing and the ocean circulation in these patterns. In Sect. 3, we also take the opportunity to show how the patterns in SSH, SST and OC relate to each other and we discuss to what extent the information in SSH, SST and OC provided by satellites enables us to monitor the mechanisms responsible for the ocean variability at climatic timescales. Section 4 summarizes the paper, reviews the future issues and draws some conclusions.

## 2 Physical Background

### 2.1 SSH Variations Deduced from the Pressure Budget of the Water Column

SSHs indicate the level of the top of ocean water columns relative to a defined reference, which is constant with time; we use in general the mean sea surface as a reference. SSH variations indicate variations in the volume of water columns and are governed by two processes: the changes in mass and the changes in density of those water columns. Both processes can be tracked through vertical pressure changes in the pressure budget. Mathematically, the pressure budget under the hydrostatic and Boussinesq approximations can be written as follows (Gill and Niller 1973):

$$\eta = \frac{1}{\rho_0 g} (p_b - p_a) + \eta_{st} \quad (1)$$

where  $\eta$  is the SSH,  $p_a$  is the sea surface atmospheric pressure,  $p_b$  is the ocean bottom pressure,  $\rho_0$  is a constant density,  $g$  is the acceleration due to gravity and  $\eta_{st}$  is the steric sea level.  $\eta_{st}$  is given by  $\eta_{st} = \frac{1}{\rho_0} \int_{-H}^0 \rho dz$  in which  $H$  is the ocean bottom depth and  $\rho$  the water density deviation from  $\rho_0$ .

The pressure budget breaks down SSH into three signals: (1) a signal which depends on the atmospheric pressure (i.e. the inverted barometer response, Wunsch and Stammer 1997), (2) a signal which depends on bottom pressure and gravity and (3) a signal which depends on the water density along the water column. The first signal is isostatic (i.e. dynamically irrelevant) on climate timescales and thus will not be analysed here. The second signal represents the mass component in sea level. It arises essentially from changes in bottom pressure caused by the water mass redistribution by the ocean circulation in response to the atmospheric forcing. This signal is the dominant component in sea level changes at high frequencies (for periods <1 months, Forget and Ponte 2015). It is much smaller at interannual and higher timescales, but it remains sizeable in particular at high latitudes (see Sect. 3). The mass signal in sea level can arise also from changes in the gravity field of the Earth (i.e. changes in local  $g$ ). These changes can be due to ongoing ice loss in ice sheets, for example, or to the current solid earth response to ice loss in ice sheets that occurred during the last deglaciation (Tamiseia 2011). However, this component in sea

level change is significant only at timescales longer than multidecadal timescales and will not be considered here. The third sea level signal in the pressure budget represents the steric component in sea level. This signal arises from changes in the sea water density due to changes in the water column temperature (thermosteric sea level) or salinity (halosteric sea level). These changes in temperature and salinity are caused by buoyancy forcing at the surface or redistribution of heat and freshwater within the ocean by the ocean circulation in response to the atmospheric forcing. The redistribution of heat and freshwater can occur through advection or diffusion (including diapycnal, isopycnal and convective mixing) such that steric sea level can be written as follows:

$$\eta_{st} = \eta_T + \eta_S = \eta_T^a + \eta_T^d + \eta_T^{BF} + \eta_S^a + \eta_S^d + \eta_S^{BF} \quad (2)$$

where subscripts  $T$  and  $S$  refer to thermosteric and halosteric sea level and  $a$ ,  $d$  and  $BF$  refer to advection, diffusion and buoyancy forcing (a more detailed explanation of the  $\eta_{st}$  budget can be found in Piecuch and Ponte 2011). Thermosteric effects ( $\eta_T$ ) dominate steric sea level variability over most of the ocean (see Sect. 3; Köhl 2014; Forget and Ponte 2015). At interannual and longer timescales, heat advection in the oceans ( $\eta_T^a$ ) plays the leading role in thermosteric sea level variability nearly everywhere, suggesting that the heat redistribution in the ocean is nearly adiabatic. However, in many locations at all latitudes, the air-sea heat flux ( $\eta_T^{BF}$ ) role is sizeable and can reach the same order of magnitude as the advection term. This is unlike the heat diffusion term which is negligible almost everywhere (except locally in the Arctic and along the margin of Antarctica close to deep water formation regions, Forget and Ponte 2015) and thus will be neglected here.

The interannual and longer time-scale variability in steric sea level is predominantly the result of internal reorganization of water masses in the ocean forced by anomalies in surface wind stress (Stammer et al. 2013). When this contribution is removed, the remaining variability is explained by buoyancy forcing anomalies (i.e. surface heat and freshwater exchanges) and the intrinsic oceanic variability spontaneously generated by the ocean circulation under the repeated seasonal atmospheric forcing (Penduff et al. 2011; Sérazin et al. 2015). It is essentially surface heat fluxes anomalies, which explain most of this residual variability (see Sect. 3). The surface heat fluxes can be written as follows:

$$\eta_T^{BF} \approx \varepsilon \frac{Q_{net}}{\rho_{ml} C_p} = \varepsilon \frac{Q_{sh} + Q_{lh} + Q_{sw} + Q_{lw}}{\rho_{ml} C_p} \quad (3)$$

where  $\varepsilon$  is the thermal expansion coefficient,  $\rho_{ml}$  is the density of the upper ocean mixed layer and  $C_p$  is its heat capacity. Surface heat fluxes are caused by the turbulent energy fluxes (sum of the sensible heat flux— $Q_{sh}$ —and latent heat flux— $Q_{lh}$ —), which are broadly proportional to the wind speed, the air-sea temperature and humidity differences. Radiative fluxes (sum of the downward solar radiative flux— $Q_{sw}$ —and the longwave radiative flux— $Q_{lw}$ —) are functions of air temperature, humidity and cloudiness.

## 2.2 SST Variations Deduced from the Heat Budget of the Upper Ocean Mixed Layer

SST from space closely reflects upper ocean mixed layer temperatures, being within 0.2 °C of upper ocean mixed layer temperatures, other than where dynamic processes drive near-surface temperature gradients (Grotsky et al. 2008). It is governed by the processes regulating the exchange of energy at the sea surface and at the bottom of the mixed layer.

These processes are both atmospheric (wind stress and buoyancy fluxes) and oceanic (heat transport by currents, vertical mixing and boundary layer depth influence). Mathematically, the heat budget can be written as follows (Deser et al. 2010).

$$\frac{\partial T}{\partial t} = \frac{Q_{\text{net,ml}}}{\rho C_p h} + \left( \overrightarrow{U}_{\text{geo}} + \overrightarrow{U}_{\text{ek}} \right) \cdot \overrightarrow{\nabla} T + \frac{W_e - W_{\text{ek}}}{h} \cdot (T - T_b) \quad (4)$$

where  $T$  is the SST,  $h$  is the mixed layer depth,  $\overrightarrow{U}_{\text{geo}}$  is the geostrophic current velocity,  $\overrightarrow{U}_{\text{ek}}$  is the Ekman current velocity,  $W_e$  is the vertical entrainment rate,  $W_{\text{ek}}$  is the Ekman pumping velocity and  $T_b$  is the temperature at depth that is entrained in the mixed layer. Ekman and geostrophic currents contribute to the heat budget of the mixed layer through horizontal advection, while entrainment velocity and Ekman pumping change the SST through vertical advection.  $Q_{\text{net,ml}}$  is the net surface energy flux which enters the mixed layer. It is the sum of the turbulent energy fluxes, the component of downward solar radiative flux, which is absorbed within the mixed layer and the longwave radiative flux. In general,  $Q_{\text{net,ml}} \approx Q_{\text{net}}$  and both terms depend on the same variables: wind speed, air-sea temperature and humidity difference, cloudiness. However, in regions of clear water and shallow mixed layer, they can be different because a non-negligible portion of the downward solar radiative flux penetrates below the mixed layer (see Sect. 3).

Thus, both SSH (through the steric sea level  $\eta_{\text{st}}$ ) and SST have a dependence on the surface heat fluxes  $\frac{Q_{\text{net}}}{\rho_{\text{ml}} C_p}$ . This common dependence is expected to give rise to correlated variability at interannual and longer timescales, in particular in response to the atmospheric forcing. In contrast, SST has a different dependency on ocean circulation from SSH: SST depends on the circulation of the upper mixed layer, while SSH depends on the circulation of the ocean from the surface down to the bottom (see, for example, Fig. 1d in Piecuch and Ponte 2011). This will result in different responses of the SST and SSH to the oceanic circulation and variability at interannual and longer timescales that are not correlated. In Sect. 3, we will explore with the use of an ocean reanalysis the complex relation which exists between SSH and SST variability through their common response to surface heat fluxes.

### 2.3 Bio-Optics of Ocean Colour

In the global ocean, phytoplankton biomass is essentially governed by the availability of light and nutrients (locally temperature and concentration of predators, i.e. zooplankton, also can play a role). A common approach to estimate phytoplankton biomass is to measure the concentration of chlorophyll (the main pigment in phytoplankton cells), because of the central role this pigment plays in photosynthesis, because it is produced uniquely by plants, and because it is easily measured, and can be estimated from satellite ocean colour observations.

Phytoplankton cells are viable in the upper layer of the ocean, where sufficient light is available and where recycled nutrients are available, and additional nutrients can be brought up from the deep oceans through upwelling, wind mixing, advection and other physical processes. The solar irradiance penetrating the ocean will be attenuated with depth due to the optical properties of pure seawater itself, and also due to the presence of particles, in particular phytoplankton cells and the chlorophyll pigment they contain.

Ocean colour is determined by the spectral variance of reflectance, defined as the ratio of upwelling irradiance (radiant flux per unit surface area,  $\text{W m}^{-2}$ ) at the surface of the ocean to the downwelling irradiance at the same depth. In satellite applications, it is also

customary to use the term remote-sensing reflectance for the ratio of upwelling radiance (radiant flux per unit surface area and unit steradian,  $\text{W m}^{-2} \text{str}^{-1}$ ) to downwelling irradiance at the surface. Both irradiance reflectance and remote-sensing reflectance, which vary with the wavelength of light considered, are functions of absorption ( $a$ ) and back-scattering ( $b_b$ ) coefficients of light, which in turn, are affected by the absorption and back-scattering properties of phytoplankton, which vary with the concentration of phytoplankton in the water, and also with the type of phytoplankton present. Though other substances, such as detritus and coloured dissolved organic material contribute to the variability in ocean colour, it is often assumed, as a first approximation, that phytoplankton may be treated as the single, independent variable that determines ocean colour in the open ocean. Remote-sensing reflectance at wavelength  $\lambda$  can be written as:

$$R_{rs}(\lambda) = f(a(\lambda), b_b(\lambda)) \quad (5)$$

where  $f$  is a function that increases with back-scattering  $b_b$  and decreases with absorption  $a$ . The function  $f$  also incorporates the effect of the angular structure in the light field on  $R_{rs}$ . As noted earlier, the absorption and back-scattering coefficients are both functions of the concentration of phytoplankton in the water, typically measured as the biomass  $B$  in chlorophyll units:

$$a(\lambda) = a_w(\lambda) + a_B(\lambda) + a_Y(\lambda) + a_X(\lambda) \quad (6)$$

and

$$b_b(\lambda) = b_{bw}(\lambda) + b_{bB}(\lambda) + b_{bX}(\lambda) \quad (7)$$

where the subscripts  $w$ ,  $B$ ,  $Y$  and  $X$  stand for pure seawater, chlorophyll concentration, concentration of coloured dissolved organic matter (sometimes called yellow substance) and particles in suspension other than phytoplankton, respectively. In the visible domain of the electromagnetic spectrum, reflectance is a small part of the solar flux that reaches just below the surface, of the order of 5 %. The rest penetrates into the ocean. The same optical properties that determine reflectance at the sea surface also dictate the rate of light penetration into the ocean. Inside the water column, the decrease in irradiance level with depth can be described using an exponential function as

$$I(z, \lambda) = I_0(\lambda)e^{-K(\lambda)z} \quad (8)$$

where  $I(z, \lambda)$  is irradiance at depth  $z$  and wavelength  $\lambda$ ,  $I_0(\lambda)$  is incident irradiance (just below the surface) and  $K(\lambda)$  is the diffuse vertical attenuation coefficient in  $\text{m}^{-1}$  (Kirk 1994). The attenuation coefficient can be expressed as

$$K(\lambda) = g(a(\lambda), b_b(\lambda)) \quad (9)$$

where  $g$  is an increasing function of both  $a$  and  $b_b$ .

Because  $K$  increases with chlorophyll, phytoplankton-rich waters display a high attenuation coefficient, and the irradiance will not penetrate as deep as in low chlorophyll waters. The photic depth (defined as the depth at which irradiance reaches 1 % of  $I_0$ ) is deeper in clear waters and shallower in waters characterized by a high chlorophyll biomass (e.g., Edwards et al. 2001).

The energy absorbed at a particular depth yields a local temperature increase with time  $t$  given by (e.g., Lewis et al. 1983)

$$\frac{\partial T}{\partial t} = \frac{1}{\rho_0 c_p} \frac{\partial I}{\partial z} \quad (10)$$

where  $T(z)$  is the temperature change (in °K) of the water due to the heating,  $c_p$  is the specific heat capacity (in  $\text{J kg}^{-1} \text{K}^{-1}$ ) and  $\rho_0$  is the density of the water ( $\text{kg m}^{-3}$ ). This equation does not account for the decrease in downwelling light with depth due to back-scattering at depth  $z$  (which does not contribute to local heating), or for heat gains by attenuation of upwelling irradiance at that depth (Edwards et al. 2001; Zaneveld et al. 1981).

Since  $I$  tends to zero below the photic depth, the heating will be confined to a layer near the surface in chlorophyll-rich waters whereas, in low chlorophyll waters, the heat energy will penetrate farther down the water column. In other words, in an oceanic region where surface chlorophyll concentration is high, the upper ocean layer will be warmer (and the deeper layer will be cooler) compared with a region where chlorophyll is absent (e.g., Sathyendranath et al. 1991; Edwards et al. 2001; Wu et al. 2007; Zhai et al. 2011).

These considerations highlight the relationship between SST and ocean colour: the optical properties have a modulating influence on the distribution of solar heating with depth, and hence on SST. Within the mixed layer, it would be reasonable to assume that the chlorophyll concentration would be uniform and equal to the value at the surface determined from ocean colour remote sensing. Where the photic depth is significantly deeper than the mixed layer, the vertical structure in chlorophyll concentration would have to be taken into account (Lewis et al. 1983).

### 3 Spatio-Temporal Patterns in SSH, SST and OC and Their Relation

In this section, we analyse the spatio-temporal patterns of SSH, SST and OC obtained from the satellite archive. To estimate these patterns, we use the ESA Climate Change Initiative (CCI) project datasets because they have been developed to be the most homogeneous and stable satellite records at interannual to decadal timescales as possible (Ablain et al. 2015; Merchant et al. 2014; Sathyendranath et al. 2016). Among SSH, SST and OC-CCI records, the SSH and SST records cover the same period: 1993–2014. In the following, we focus our analysis on this period 1993–2014 because it is the longest period covered by the CCI datasets. In addition to satellite datasets, we use an update of the analysis of ocean subsurface temperature and salinity by Ishii and Kimoto (2009) to estimate the steric effect in SSH variability. This analysis is based on temperature and salinity data from the World Ocean Database and Atlas, the Global Temperature-Salinity in the tropical Pacific from IRD (l'Institut de Recherche pour le Développement, France) the Centennial in situ Observation-Based Estimates sea surface temperature and Argo profiling floats data. This in situ measurements record has become almost global since 2006 for the upper 2000 m (Argo array). Before 2006, the historical in situ measurements are sparse (time, space and depth), and they are sparser for salinity than for temperature profiles. In particular, a large fraction of the deep/abyssal ocean (below 700 m depth before 2006 and below 2000 m depth after 2006) still lacks in situ measurements. We also make use of an ocean reanalysis to unravel the role of the atmospheric forcing and the ocean circulation in the patterns of SSH, SST and OC. The reanalysis used here is the ECCO (Estimating the Circulation and Climate of the Ocean)—Production version 4 Release 1 solution (Forget et al. 2015; Forget and Ponte

2015), hereafter referred to simply as ECCO. This product represents a model solution that has been constrained to observations (e.g., satellite altimetry, Argo floats and historical hydrography) based on the method of Lagrange multipliers. The optimization is achieved by making iterative adjustments to the initial conditions, boundary conditions and internal model parameters (consult Wunsch and Heimbach 2007, for more details on the general procedure). This solution covers the period 1992–2011. The ocean model setup is global, including the Arctic, and is fully coupled to an interactive sea ice and snow model. The spatial grid has a nominal 1-degree horizontal resolution, telescoping to 1/3-degree in the tropics and effectively 40 km in the Arctic, and uses 50 vertical levels. Initial-guess bulk-formula surface forcing is taken from the Interim European Centre for Medium-Range Weather Forecasts Reanalysis (ERA-Interim) of Dee et al. (2011) and iteratively adjusted as outlined above. The model also uses parameterization schemes to incorporate the effects of geostrophic eddies, vertical mixing and salt plumes (see Forget et al. 2015, for more details on this solution). We have chosen ECCO v4 because it has been shown to fit well to observations of SSH (Forget and Ponte 2015), in situ temperature and salinity (Forget et al. 2015), SST (Buckley et al. 2014) as well as other ocean circulation and climate variables (e.g., Piecuch et al. 2015).

In this paper, we focus on the climate fluctuations of the ocean and we analyse their signature on the SSH, SST and OC variables. In several regions, such as western boundary current regions, individual meso-scale eddies can generate substantial variability in ocean variables and mask the underlying climate fluctuations. To remove this noise from eddies, we perform a spatio-temporal smoothing on the SST and SSH data (see Sect. 3.3.2 for OC analysis) which filters out the smaller spatial scales and the shorter timescales consistently in observations and model. The spatio-temporal smoothing consists in applying first a 30-day boxcar window and then a spatial Gaussian filter which removes the variability on scales smaller than  $3^\circ$ . As in Forget and Ponte (2015), we have chosen 30 days for the temporal smoothing scale because it corresponds to the longest repeat cycle among observation datasets, and thus it enables us to get full maps of each observation dataset before performing the spatial smoothing. For the spatial smoothing scale, we have chosen  $3^\circ$  because it enables us to separate properly the ocean mesoscale, which relates to the baroclinic Rossby radius of deformation that is of the order of hundreds of km, from the ocean large-scale climate fluctuations driven by the atmospheric forcing, which are of the order of thousands of km (Forget and Ponte 2015).

In the following sections, the spatio-temporal patterns of SSH, SST and OC at inter-annual and decadal timescales are analysed in terms of standard deviation and trend of the time series. For SSH and SST data, the linear trend over 1993–2011 is estimated simultaneously with the seasonal cycle from monthly time series. After removing the trend and the seasonal cycle, we apply a 13-month Hanning window to remove remaining intraseasonal signals and then we estimate the standard deviation of the residual time series. For OC data, the linear trend over 1998–2010 is estimated based on monthly chlorophyll anomalies

### 3.1 Sea Level and How it Relates to Ocean Mass, Temperature and Salinity

#### 3.1.1 Regional Variations

SSH observations from the CCI sea level dataset show considerable interannual variability (Fig. 1a). This variability is maximum within the tropics. Temperature and salinity

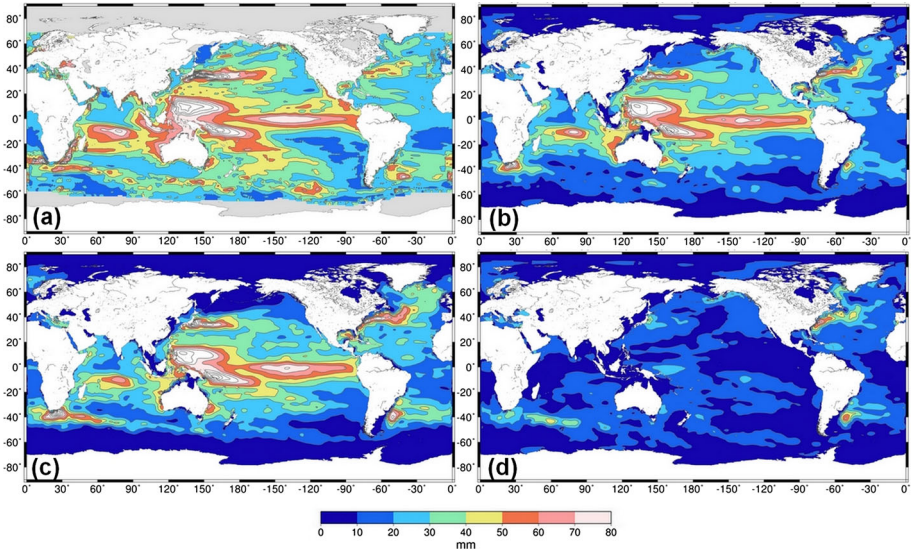


**Fig. 1** **a** Standard deviation in SSH ( $\eta$ ) from the CCI sea level dataset. **b–d** Standard deviation in, respectively, steric height ( $\eta_{\text{Steric}}$ ), thermosteric height ( $\eta_T$ ) and halosteric height ( $\eta_S$ ) from an update of Ishii and Kimoto (2009). Heights are in mm. Note that thermosteric and halosteric data have large uncertainties in regions where the in situ temperature and salinity observations are poor like in the southern ocean before 2006

observations have a very sparse coverage in the Arctic and do not allow evaluation of the steric effect in this region. But, for the rest of the ocean, they show that most of the interannual variability in sea level is dominated by the interannual variability in steric sea level (Fig. 1b). This result is confirmed by independent data from space gravimetry over the period 2004–2014. Indeed, the Gravity Recovery and Climate Experiment (GRACE) mission, which measures the time varying gravity field of the Earth, provides continuous estimates of the ocean bottom pressure since 2004. These estimates confirm that ocean bottom pressure interannual variability is smaller than the steric variability by an order of magnitude except at high latitudes and in shallow shelf seas ( $>60^\circ\text{N}$  and  $<55^\circ\text{S}$ , Piecuch et al. 2013; Ponte and Piecuch 2014).

At mid and low latitudes, the steric sea level signal is essentially due to temperature changes (Fig. 1c). Salinity changes play only a local role (Fig. 1d), but this role can be sizeable in several regions like the Eastern Indian Ocean (Llovel and Lee 2015) or the North Atlantic (Wunsch et al. 2007; Köhl 2014; Forget and Ponte 2015).

The picture is similar for the trends in sea level as for the standard deviation. They are largely dominated by the steric effect (Fig. 2a, b). The halosteric effect is much smaller than the thermosteric effect, but it is sizeable in many regions and should not be neglected (Fig. 2c, d). Interestingly, in the few regions where the halosteric signal is sizeable, like in the southern tropical Pacific, its effect tends to compensate the thermosteric effect. Such compensation suggests nearly adiabatic transport of the water masses in these regions (an example of such adiabatic transport is heaving of the water column) as suggested by previous authors (e.g., Wunsch et al. 2007; Durack et al. 2014).

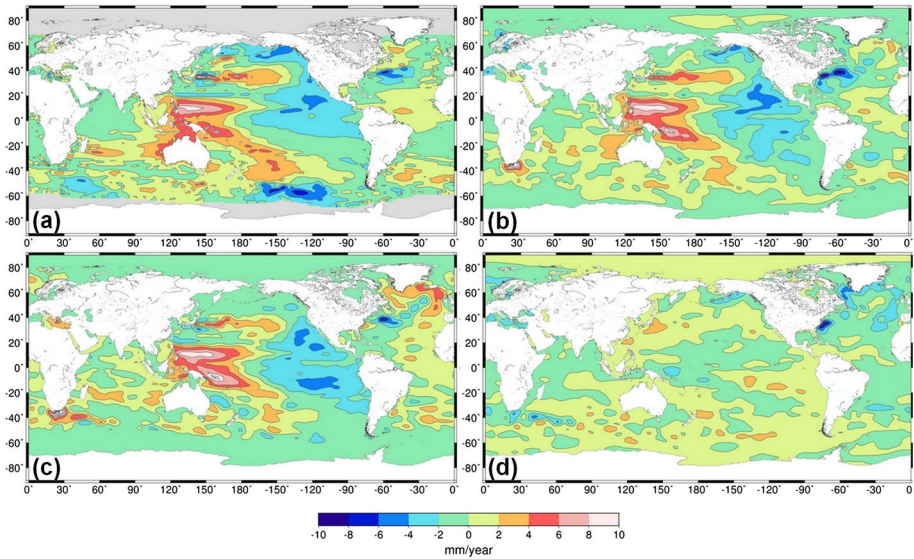


**Fig. 2** **a** Trends over 1993–2011 in SSH ( $\eta$ ) from the CCI sea level dataset (Ablain et al. 2015). **b–d** Trends over 1993–2011 in, respectively, steric height ( $\eta_{\text{Steric}}$ ), thermosteric height ( $\eta_{\text{T}}$ ) and halosteric height ( $\eta_{\text{S}}$ ) from an update of Ishii and Kimoto (2009). Trends are in mm/year. Note that thermosteric and halosteric data have large uncertainties in regions where the in situ temperature and salinity observations are poor like in the Southern Ocean before 2006

### 3.1.2 The Effects of Wind Stress and Surface Buoyancy Fluxes

The ECCO model estimate shows similar patterns in SSH variability and trends as those obtained from the CCI observations (Figs. 3a, 4a). The ECCO estimate of the ocean bottom pressure (Figs. 3c, 4c) and of the steric effect (Figs. 3b, 4b) corroborates the notion that SSH variability and trends are dominated by the steric effect in general. At high latitudes, in the polar oceans where altimetry data are not available, ECCO also provides SSH estimates. In these regions, the SSH variability and trends appear to be substantial and actually dominated by the mass signal (Figs. 3c, 4c). This mass signal in the Arctic and in the Southern Ocean has been confirmed by GRACE observations since 2004 (Purkey et al. 2014; Makowski et al. 2015). It is the result of the barotropic circulation caused by wind forcing (Frankcombe et al. 2013; Volkov and Landerer 2013; Volkov 2014; Peralta-Ferriz et al. 2014; Fukumori et al. 2015; Makowski et al. 2015). In the Arctic, ECCO shows that the steric effect is actually sizeable and should not be neglected in comparison with the mass signal. This steric effect has a significant halosteric component coming from the variability of the freshwater inputs in the Arctic and the sea ice (see Fig. 4 in Köhl 2014, which suggests that both mixed layer processes and heaving of isopycnals contribute to interannual halosteric variability in the Arctic). At low and mid latitudes, ECCO confirms that the sea level variability and trends are almost entirely of thermosteric origin with some local halosteric effect, which tends to compensate the thermosteric effect as in observations.

An advantage of reanalyses over observations is that they allow unambiguous identification of the anomalous forcings, which are responsible for the interannual variability and the trends in SSH. In this subsection, we use perturbation experiments based on the ECCO model setup to distinguish the influences of wind stress and buoyancy exchanges on sea

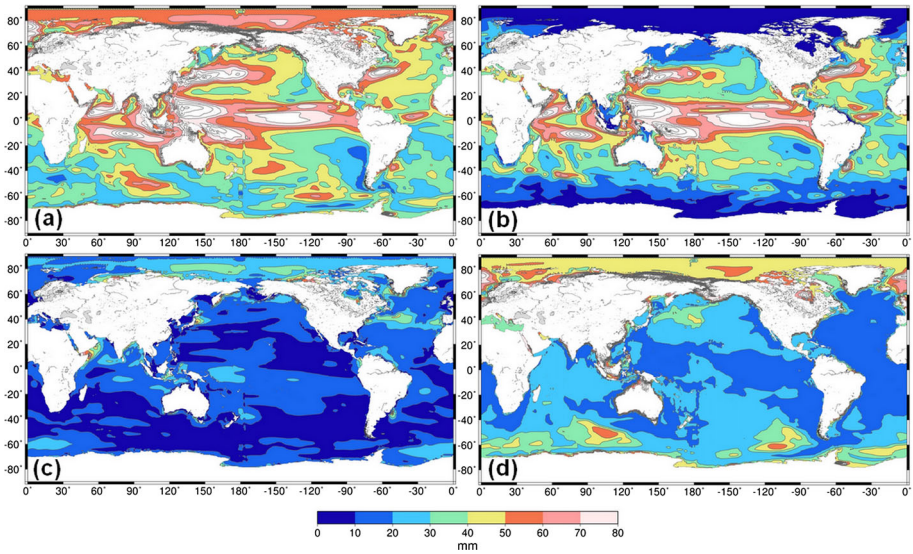


**Fig. 3** a–d Standard deviation in, respectively, SSH ( $\eta$ ), thermosteric height ( $\eta_T$ ), halosteric height ( $\eta_S$ ) and bottom pressure ( $p_b$ ) from ECCO version 4. Heights are in mm

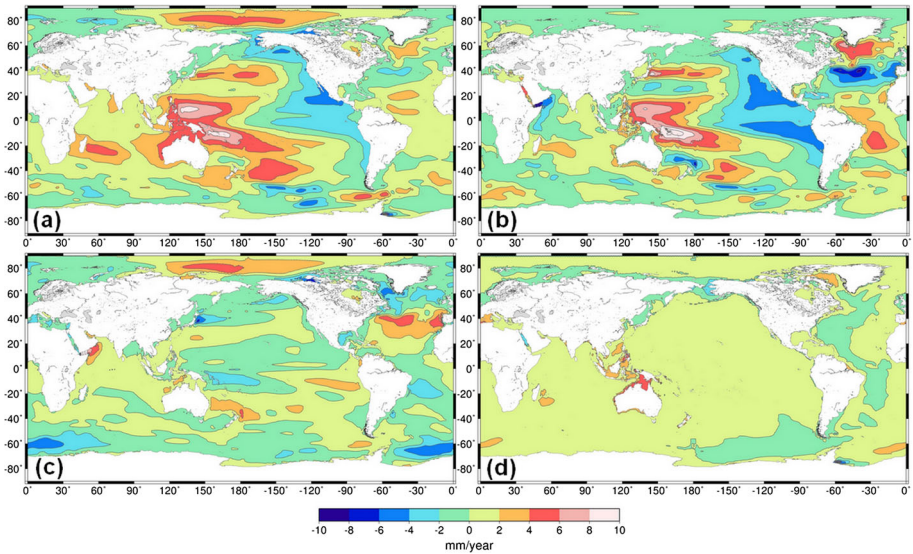


**Fig. 4** a–d Trends over 1993–2011 in, respectively, SSH ( $\eta$ ), thermosteric height ( $\eta_T$ ), halosteric height ( $\eta_S$ ) and bottom pressure ( $p_b$ ) from ECCO version 4. Trends are in mm/year

level. This set of experiments is described more extensively by Forget and Ponte (2015). In more detail, each member of that set employs different surface boundary conditions. In each run, a common forcing component was prescribed, which comprised both fully variable surface buoyancy exchanges and a climatological mean seasonal cycle in wind stress. What differed between the simulations was that interannual changes in the wind

stress were or were not turned off over the global ocean. The difference between these two experiments (shown in Figs. 5a, 6a) represents the oceanic response to interannual and decadal wind stress changes; the experiment without interannual or decadal wind stress changes (but retaining the common forcing component; shown in Figs. 5b, 6b) reflects the ocean's adjustment to interannual and decadal changes in buoyancy exchanges as well as any nonlinear intrinsic changes (cf. Penduff et al. 2011; Piecuch and Ponte 2012)

The perturbation experiments reveal that SSH variability is essentially forced by surface wind stress anomalies (see Fig. 5a, c and also Stammer et al. 2013; Forget and Ponte 2015). The remainder variability, which is forced by anomalous surface fluxes of buoyancy along with any nonlinear intrinsic variability (cf. Penduff et al. 2011), is in general significantly smaller except in some regions (Fig. 5b, d) such as the region of the Antarctic circumpolar current (ACC), in the Kuroshio extension, in the Arctic, in the North Atlantic, in the North Pacific and in the tropical Pacific, confirming earlier results from Thompson and Ladd (2004), Cabanes et al. (2006) and Piecuch and Ponte (2012, 2013).

In the case of SSH trends over 1993–2011, the perturbation experiments reveal that both wind stress forcing and buoyancy forcing play a leading role in SSH trends but in different regions. In the tropics, it is the wind stress anomalies which are responsible for the SSH trends (Fig. 6a). Indeed, the large positive pattern in the western tropical Pacific has been associated with a deepening of the thermocline in response to trade wind intensifications, probably linked to the negative phase of the Pacific decadal oscillation in recent decades (Timmermann et al. 2010; Merrifield 2011; McGregor et al. 2012; Qiu and Chen 2012; Meyssignac et al. 2012; Moon and Song 2013; Meehl et al. 2013; Palanisamy et al. 2015). In the extra tropics, the SSH trends are essentially driven by the buoyancy forcing (Fig. 6b), while the wind stress forcing contribution is smaller but remains significant in

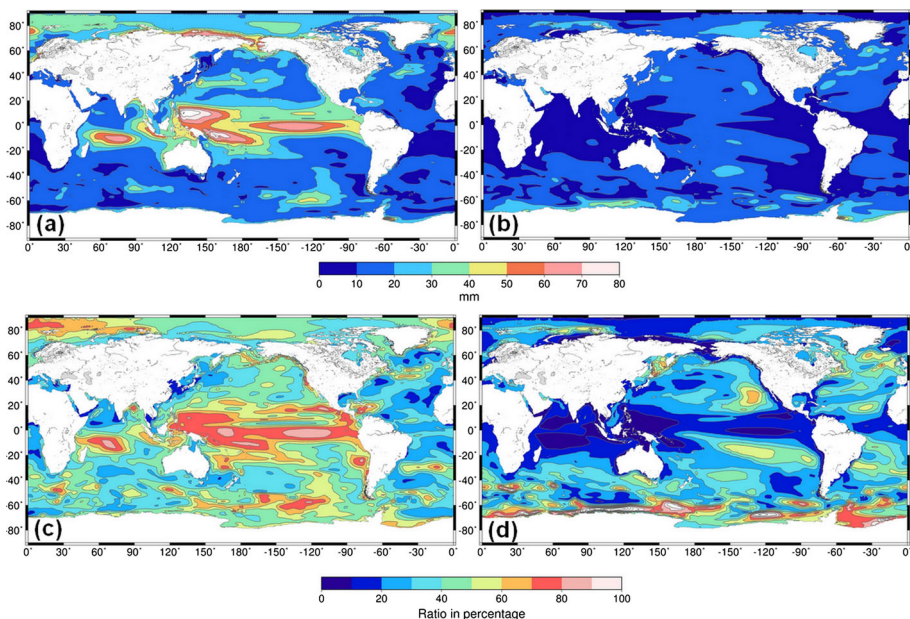


**Fig. 5** Interannual variability in  $\eta$  due to wind stress (a) and to buoyancy forcing (b) from ECCO version 4. (See the text for the definition of  $\eta$  due to wind stress and to buoyancy forcing). Ratio of the interannual variability in  $\eta$  due to wind stress (c) and buoyancy forcing (d) over the interannual variability in total  $\eta$

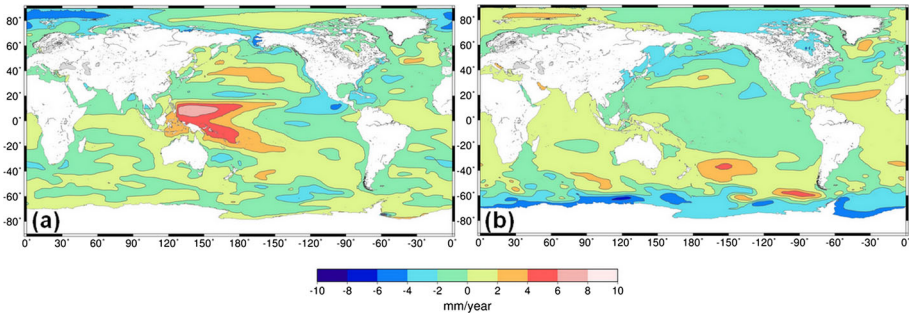


**Fig. 6** Trends in  $\eta$  between 1993 and 2011 (in mm/year) from ECCO version 4. **a** Contribution due to wind stress; **b** contribution due to buoyancy forcing

several regions (such as the North and South Pacific and the Arctic, see Fig. 6a, b). Note that the trends in SSH driven by the buoyancy forcing are positive all over the ocean reflecting the general warming of the ocean. Interestingly, they are maximum in the subtropical gyres and in the North Atlantic subpolar gyre.

### 3.2 SST and How it Relates to Sea Level and Ocean Temperature and Salinity

#### 3.2.1 Regional Variations

Interannual variability in SST is presented in Fig. 7 as the standard deviation of de-seasonalised, de-trended monthly SST anomalies. Very low SST variability at high latitudes in areas of perennial sea ice reflects the damping of variability in SST by the freezing and melting of that sea ice: in the SST data set, SST is set to the freezing temperature of sea water where the ocean is ice covered. Variability is greater in areas of seasonal sea ice, where variations in sea ice extent are reflected also in SST.

In the extra tropics poleward of sea ice, the variability in monthly SST is seen to be relatively high, typically of order 1 K. Much of the large-scale development of SST anomalies in the extra tropics is driven by large-scale reorganization of atmospheric circulation anomalies. Atmospheric variability with timescales longer than  $\sim 10$  days is effective at driving SST anomalies that reflect the temperature of the upper mixed layer, because of the large thermal inertia of the upper ocean mixed layer (Frankignoul and

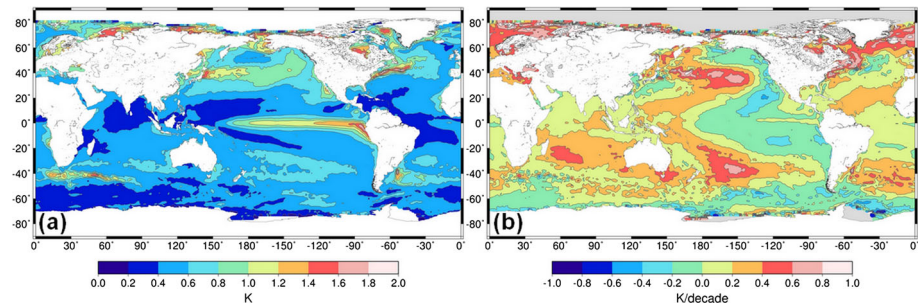


**Fig. 7** Variability and trends in SST from the CCI dataset (Merchant et al. 2014). **a** Standard deviation in K. **b** Linear trend in over 1993–2011 in K per decade

Hasselmann 1977; Deser et al. 2003). (Note that, however, SST can respond strongly to higher frequency atmospheric variability when the depth of the response is shallow, as in diurnal variability.) The large-scale nature of atmospheric teleconnection patterns is imprinted upon the SST anomaly field essentially via the surface energy fluxes and Ekman currents (e.g., Cayan 1992; Marshall et al. 2001; Visbeck et al. 2003). Spatial variations in mixed layer depth (which themselves reflect the recent history of wind stress) modify the effective thermal inertial and also play a role in determining the magnitude of the SST anomalies.

Across much of the tropics, variability in monthly SST is low,  $<0.5$  K. The clear exception is the equatorial Pacific Ocean, where SST variability  $>1.5$  K is present eastwards of  $180^\circ\text{W}$ , associated with the El Niño Southern Oscillation (ENSO). ENSO is a coupled mode of variability, in which large-scale atmospheric circulation anomalies develop in close interaction with the SST variability, in contrast to extratropical anomalies (e.g., Deser et al. 2010).

Local processes such as upwelling, entrainment and lateral advection also contribute to SST variability. For example, vertical advection plays a prominent role along the coastal and equatorial upwelling zones, with variability being wind-driven. Horizontal advection is important along the western boundary current regions (e.g., the Gulf Stream and Kuroshio Current). Oceanic processes also play an indirect role in SST variability by affecting the depth of the upper ocean mixed layer.

The trends in SST over the period are relatively uniform around  $0.3$  K decade $^{-1}$  across much of the Atlantic and Indian Oceans. The North Atlantic, including the Barents Sea, the sub-Greenland gyre and Labrador Sea, shows a warming trend exceeding  $0.5$  K decade $^{-1}$ . Across the Pacific Ocean, the SST trend largely reflects the change in the tendency of the Pacific Decadal Oscillation over the period (Fig. 7a), as previously noted with respect to SSH.

### 3.2.2 The Effect of Surface Heat Fluxes and Ocean Transport

The ECCO model estimate shows generally similar patterns in SST variability as those obtained from the CCI observations (Fig. 8a), except at mid latitudes and in the Southern Ocean where it tends to underestimate the SST variability notably in eddy active regions (in the Kuroshio and Gulf Stream extensions, the Malvinas current and the Agulhas current). It shows also generally similar patterns in SST trends (Fig. 9a) except in the North Atlantic (from the Gulf Stream extension to the Barents sea) and in the eastern part of the north Pacific where trends are underestimated by a few tenths of K/decade and in the north-east Indian Ocean and China sea where trends are overestimated by a few tenths of K/decade.

As for SSH, we use ECCO output to infer the role of surface heat fluxes and ocean transport divergences in SST variations. We integrate vertically the upper ocean temperature budget (Eq. 7 in Piecuch and Ponte 2012) over a constant climatological mixed layer depth computed for each grid cell. The role of surface heat fluxes on SST is diagnosed by calculating the changes in SST due to the surface heat forcing term  $\frac{Q_{\text{net,ml}}}{\rho C_p h}$ . The ocean transport divergences effect is diagnosed by calculating the changes in SST due to the sum of the advection and diffusive terms. This form of the upper ocean temperature budget does not distinguish between Ekman and geostrophic transport contributions as in Eq. (4). However, it allows the same separation of SST in terms of surface heat forcing and ocean transport divergences as for steric sea level (Sect. 3.1). In that sense, it allows us to

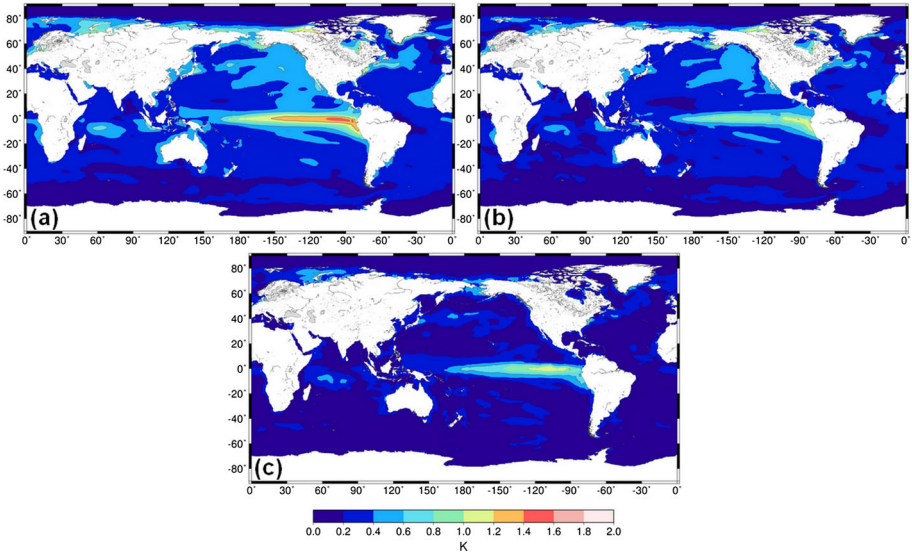


**Fig. 8** a Standard deviation in SST from ECCO. b standard deviation in SST due to the surface heat fluxes (after removing the cancellation part with ocean transport divergences). c Standard deviation in SST due to the ocean transport divergences (after removing the cancellation part with surface heat fluxes)

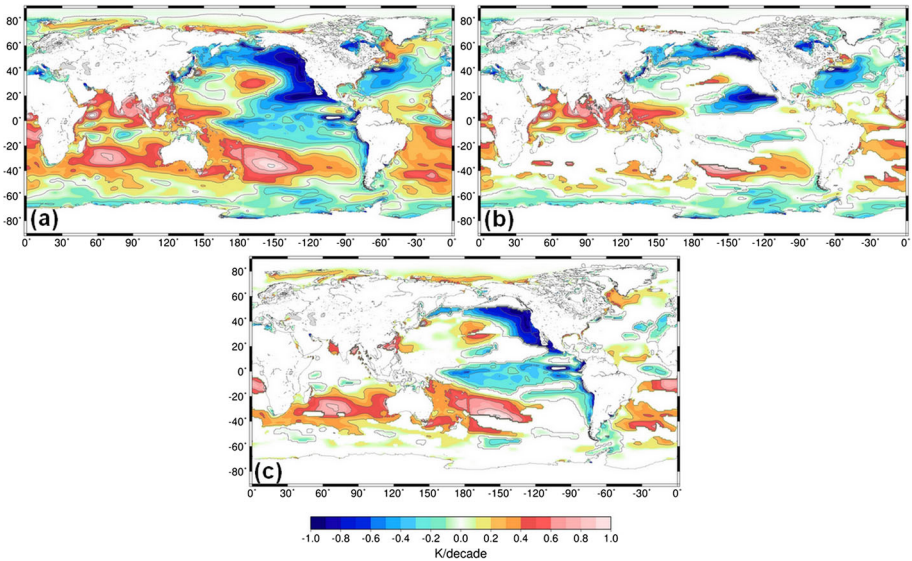


**Fig. 9** Same as Fig. 8 but for trends

compare easily between upper ocean heat and steric sea level budgets, being able to infer whether surface heat fluxes or ocean transport divergences are more or less important for upper ocean heat or steric sea level changes.

Both standard deviation patterns in SST due to surface heat flux and ocean transport divergences are very similar (see Fig S1a, b in the supplementary material). They show

high variability in the tropics and upwelling regions and low variability at higher latitudes with a minimum in the Arctic Ocean north of 80°N and in the Southern Ocean. The amplitudes of both standard deviation maps are also significantly higher than the standard deviation of the SST map almost everywhere: this is a result of integrating the ocean temperature budget over time. The effect of surface heat fluxes on SST is opposite to the effect of ocean transport divergences almost everywhere and they tend to cancel out (see Fig S1a, b). However, the cancellation of surface heat fluxes effect with ocean transport divergences effect is not exact and gives rise to SST variability. Figure 8b and c shows the standard deviation of the residual in SST due to surface heat fluxes and ocean transport, respectively, after removing the cancellation part (see also Fukumori and Wang 2013). Figure 8b shows that the interannual variability in SST due to the surface heat flux forcing is larger almost everywhere except in the tropical Pacific where ocean transport divergences play a similar role to surface heat fluxes in the local SST variability.

The same compensation process between surface heat fluxes and ocean transport divergences effects on SST occurs at longer timescales. The trend pattern in SST due to surface heat flux and ocean transport is very similar and tends to cancel out each other (see Fig. S2a, b in the supplementary material). Trends in SST due to surface heat fluxes are very large in the tropics and very low in boundary current regions and at high latitudes (Fig. S2a), while trends in SST due to ocean transport divergences are opposite in the same regions reflecting that the ocean gains most of the heat in the tropics and transports it to higher latitudes where it is released to the atmosphere or buried in the deeper layers of the ocean. However, the effect of surface heat fluxes and ocean transport divergences on SST trends does not fully cancel out everywhere. Figure 9b, c shows the residual in SST trends due to excess surface heat fluxes or ocean transport divergences, respectively, after removing the cancellation part. Figure 9b shows that surface heat fluxes dominate over ocean transport divergences and explain the SST trends in the tropical Indian Ocean, in the western tropical Pacific Ocean, in the North Pacific and North Atlantic subtropical gyres. It also dominates in the North Atlantic subpolar gyre and on the southern edge of the South Pacific subtropical gyre. In all upwelling regions (California current, Humbolt current and to a lesser extent in the Benguela current), it is the ocean transport divergences effect which dominates and explain the SST trends. In the eastern tropical Pacific, in the Indian and South Pacific subtropical gyres and in the North Atlantic subpolar gyre, it also dominates. Interestingly enough, the dominance of the ocean transport divergences over the surface heat fluxes, which explain the negative trends in SST in the California current, the Humbolt current and the eastern tropical Pacific, is consistent with the increase in cold deep water entrainment in these regions in response to increasing trade winds associated with the decreasing Pacific Decadal Oscillation (PDO) over the period 1993–2011.

The case of the western tropical Pacific region where the SST trends are dominated by surface heat fluxes warrants further discussion. At first sight, this result seems inconsistent with Fig. 6, which indicates positive SSH trends in this same region due to wind forcing (see Sect. 3.1.2). But there is a possible interpretation. The time-mean SST budget in the western tropical Pacific Ocean is a balance between strong increase due to surface heat fluxes and strong decrease due to ocean transport divergences (see Fig. S2). Over the study period, well-reported-on wind stress changes act to reduce the magnitude of that background ocean transport divergence contribution, making it less negative (and resulting in the steric sea level rise in this area). This results in their being an excess of surface heat forcing contribution (or deficit of ocean transport divergence contribution), which leads to the result in Fig. 9 that the western tropical Pacific SST trends are attributed to surface heat flux forcing.

### 3.2.3 Comparison with SSH Variability

At interannual timescales, SSH and SST show a fairly large common variability in the tropical band and in upwelling regions. Figure 10a shows the correlation map of SST and SSH detrended interannual time series computed from the CCI observational datasets. The correlation is higher than 0.7 in most of the tropics, in the California current, the Humbolt current and in the Canary current. In the Benguela current, the correlation is not significant, but it is potentially because this narrow coastal current is not well sampled by satellite altimetry and its variability in SSH is not captured properly by the CCI product (Note that the correlation is significant and high in the Benguela current in the ECCO estimate which support this hypothesis—see Fig. 10b). In the extra tropics, the correlation is in general non-significant except south-east of Greenland and in some local eddies in the Antarctic circumpolar current, in the Kuroshio extension and in the Gulf Stream. The ECCO estimate confirms this global picture and shows a similar pattern in the correlation map for SST and SSH as in the CCI correlation map (see Fig. 10b). The one difference between the ECCO correlation map and the CCI correlation map is that the ECCO estimate shows actually significant correlations in large regions of the extra tropics, but these correlations are low and below 0.6 in general.

To get insights into the cause of the common variability in SSH and SST, we correlate the detrended interannual time series of SST with the wind-driven SSH response (see Fig. 10c) and with the buoyancy-forced SSH response (see Fig. 10d). Figure 10c and d shows that, in general, SST is more closely related to the buoyancy-forced sea level response than it is to either the total (wind + buoyancy) sea level or the wind-driven sea level. In particular, for buoyancy-driven sea level, the average correlation coefficient between sea level and sea surface temperature is 0.55 and the correlation coefficient is

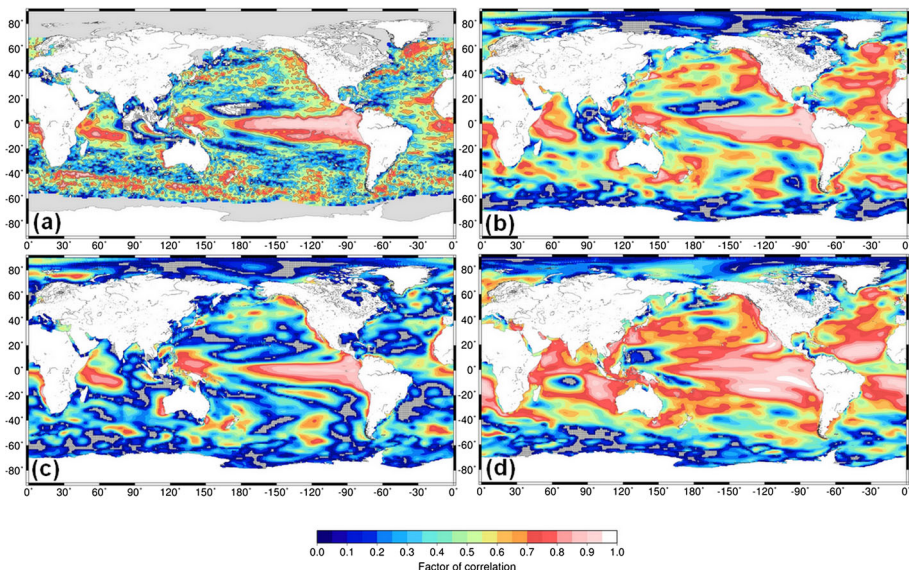


**Fig. 10** Correlation coefficient between SST and SSH for CCI (a), between SST and total SSH for ECCO (b), between SST and the wind forcing driven SSH (c), between SST and the buoyancy-forced SSH (d). Only positive correlations are shown because actually no significant negative correlation between SST and SSH was found

significant over 68 % of the global ocean. These same numbers for the wind-driven sea level are 0.25 and 29 %, respectively. And these same numbers are 0.49 and 63 % for the fully forced (wind + buoyancy-driven) sea level, respectively. The reason for the high correlation between SST and buoyancy-forced SSH is that the SST variability is dominated in most regions of the ocean by the SST response to surface heat fluxes (see Sect. 3.2.2; Fig. 8b) and that in many regions also surface heat fluxes dominate over freshwater fluxes effects in the buoyancy-forced sea level response. As a result, surface heat fluxes appear as the main cause for the common variability in SSH and SST. In a few regions, this statement does not hold. In regions where the freshwater effect on the buoyancy forcing is dominant over the heat flux effect, like in the Pacific warm pool or in the Arctic region, the correlation of buoyancy-forced sea level with SST is not significant (see Fig. 10c). In the tropics and in the upwelling regions, the wind stress is also a cause of sizeable common variability in SST and SSH along with the surface heat flux (see Fig. 10d). This is because wind stress variability in the tropics generates at the same time a zonal pressure gradient and a zonal tilt in the thermocline, which make, respectively, sea level and SST vary in phase in this region.

The picture is different for trends in SSH and SST. The relationship between SST and buoyancy-forced sea level is somewhat less clear for trends than it is for interannual to decadal timescales. For example, the correlation coefficient between the spatial patterns in SST (Fig. 9a) and SSH (Fig. 2b) is 0.32, between SST and wind-driven SSH (Fig. 6a) is 0.15, and between SST and buoyancy-forced sea level (Fig. 6b) is 0.28. This means that at long timescales, while SST is more correlated with buoyancy-driven sea level than it is with wind-driven sea level, SST is even more correlated (but still modestly so) with the total sea level. This indicates that probably the relationship between SST and buoyancy-forced sea level is quite complex in general, and probably depends critically on timescale, among other factors. One striking feature when looking at Figs. 9a and 6b is that, out of the tropics, the SST pattern seems quite similar to the buoyancy-forced sea level except around Greenland. Around Greenland, sea level trends are more subdued, while surface temperature trends are more pronounced. This decoupling is potentially due at least in part to freshwater fluxes and halosteric sea level changes in this region. Indeed, models suggest that such salinity effects on sea level are important in this region and act to compensate and offset sea level changes due to temperature effects (i.e. thermosteric height, Köhl 2014). In the eastern tropical Pacific, the negative SST trends are in phase with the negative SSH trends which are essentially caused by wind stress. This is consistent with the increasing trade winds associated with the decreasing PDO since the late 1970s. Another interesting region is the Arctic (and to a lesser extent the south of the Southern Ocean) where the SST pattern does not correlate with any sea level pattern. The reason is probably that mass (bottom pressure) trends probably play an important role in sea level trends as well as the halosteric effects and hence make the SSH trends independent of the SST trends.

### 3.3 Ocean Colour and How it Relates to SST and SSH

#### 3.3.1 General Principles

To investigate how ocean colour relates to SST and SSH, we must first understand the dominant processes driving the biophysical interactions, which include the constraints on phytoplankton dynamics imposed by the physical environment, and also the feedback mechanisms by which phytoplankton could modify their environment.

In the open ocean waters of the tropics and subtropics, light is plentiful all-year round and phytoplankton biomass increases when nutrients become available in the mixed layer through various vertical processes, such as wind mixing and upwelling. The transport of cold waters from depths to the surface, carrying nutrients with them, reduces SST. In such cases, a decrease in SST can be considered a proxy for nutrient supply. These regions are therefore characterized by a negative correlation between SST and chlorophyll concentration.

In contrast, in high latitudes, light availability is the dominant driver: phytoplankton biomass shows a clear seasonality (tied to the annual solar cycle), and surface nutrients are generally replenished by deep-mixing in winter. In these regions, the seasonal changes in light at the sea surface are accompanied by seasonal warming of the waters, such that an increase in SST may be taken here to be a proxy for increase in available light.

Sea level variations can reflect alterations in ocean circulation and ocean density, occurring in response to changes in wind forcing, ocean warming and changes in water and ice mass exchange between the land and the oceans (Church et al. 2013). Some of these processes form zones of convergence and divergence in the ocean, which are characterized by enhanced water column stratification and upwelling, respectively. In the tropics and subtropics, zonal wind stress patterns cause convergence zones and increase sea level (Palanisamy et al. 2015). Such zones are also characterized by deep thermoclines and low nutrient availability, which are unfavourable for phytoplankton production (Kahru et al. 2010); a negative correlation between SSH and chlorophyll concentration can be observed (Turk et al. 2001). In high latitudes, oceanic convergence zones also show an increase in SSH, but the conditions may still favour phytoplankton production due to enhanced upper ocean light availability and supply of nutrients from winter mixing. In these regions, positive correlations can be found between SSH and chlorophyll (e.g., Wilson and Coles 2005; Brewin et al. 2014).

### 3.3.2 Correlation Analyses Based on CCI Datasets

Ocean colour observations from the OC-CCI dataset show high inter-annual variability (Fig. 11a) at high latitudes and in coastal upwelling highly productive regions, whereas low variability is observed in the oligotrophic gyres (where phytoplankton production is minimum). Trends based on monthly chlorophyll anomalies are shown in Fig. 11b. Correlation coefficients calculated using monthly means and monthly anomalies over the period 1998–2010 between chlorophyll (OC-CCI) and sea level (SL-CCI), and between chlorophyll (OC-CCI) and SST (SST-CCI) are presented in Fig. 12. Although the correlation between chlorophyll and SSH tends to be weaker when compared with that between chlorophyll and SST, they display similar regional patterns throughout most of the global oceans. The tropics and subtropics typically show negative correlations (i.e. chlorophyll is low when SST and SSH are high), whereas the high latitudes typically show positive correlations (i.e. chlorophyll is high when SST and sea level are high), as expected from the rationale presented above. In high latitudes, positive correlations between chlorophyll and SST are weaker when monthly anomalies (representative of inter-annual variability) are used compared with monthly means (when the seasonality has not been removed), but they show similar patterns (Fig. 12). The correlation patterns displayed in the tropics, subtropics and high latitudes are consistent with previous studies, which have been carried out for different time periods and different satellite sensors (e.g., Wilson and Coles 2005; Brewin et al. 2012, 2014; Siegel et al. 2013). This consistency suggests that the patterns are independent of the time period selected for the

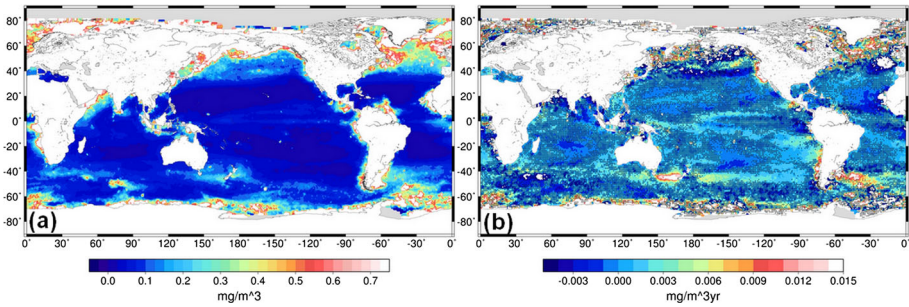


**Fig. 11** **a** Standard deviation in chlorophyll concentration. **b** Linear trend in chlorophyll concentration anomalies calculated over the period 1998–2010. Only the linear regression coefficients, which are significant at the 95 % confidence level, are shown in colour. Non-significant linear regression coefficients are in grey

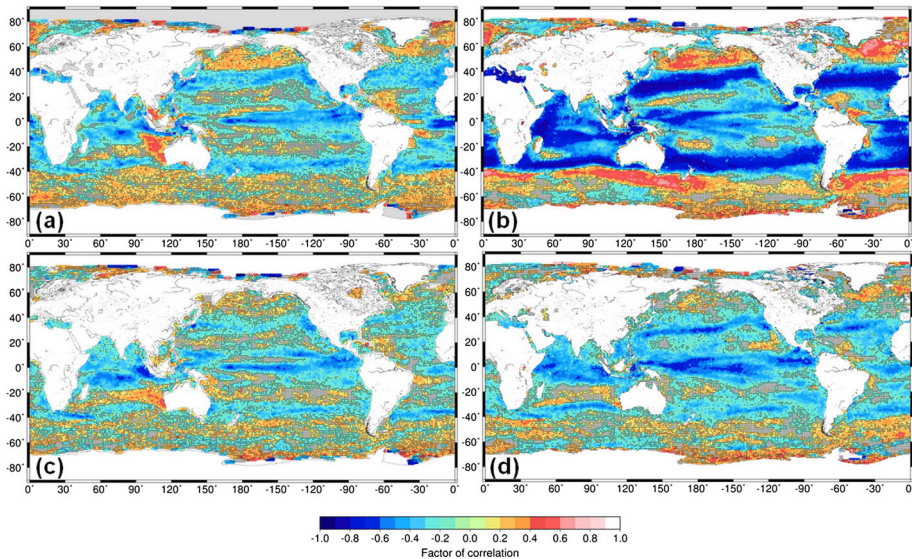


**Fig. 12** Relationships between OC and SSH and between OC and SST over the period 1998–2010. **a** Correlation analysis between monthly means of chlorophyll concentration and SSH; **b** Correlation analysis between monthly means of chlorophyll concentration and SST; **c** Correlation analysis between monthly anomalies of chlorophyll concentration and SSH; and **d** Correlation analysis between monthly anomalies of chlorophyll concentration and SST. Chlorophyll concentration data are from OC-CCI, SSH data are from SL-CCI, and SST data are from SST-CCI. Only the correlation coefficients, which are significant at the 95 % confidence level, are shown

analysis and of differences in chlorophyll-retrieval and atmospheric correction algorithms used (Brewin et al. 2014; note also that OC-CCI product includes data from three sensors—SeaWiFS, MODIS and MERIS—which have been processed using SeaDAS—Fu et al. 1998—and POLYMER atmospheric correction algorithms—Steinmetz et al. 2011—and show a significant increase in data coverage (Sathyendranath and Krasemann 2014; Racault et al. 2015; Sathyendranath et al. 2016).

### 3.3.3 Regional Variations

Other considerations have to be invoked to explain variations superimposed on these large-scale, latitudinal patterns. Some of these regions are examined more closely below.

**3.3.3.1 High Latitude HNLC Regions** In certain regions that are known as high nutrient-low chlorophyll (HNLC) regions (Boyd et al. 2007), some trace nutrients (notably iron) may remain low, even when other nutrients such as nitrogen, phosphorus and silica are available, limiting phytoplankton production. In HNLC regions in high latitudes (including parts of the Pacific and the Southern Ocean), the correlation between chlorophyll and SST may become weak or negative, indicating that phytoplankton growth is predominantly limited by nutrient availability rather than light availability. Based on observed relationships between chlorophyll and SST and chlorophyll and SSH, Le Quéré et al. (2002) estimated that in the Southern Ocean between 40°S and 65°S, 44 % of the total primary production was predominantly light limited, and 10 % was driven by changes in stratification and nitrogen supply, which in turn was associated with changes in SST. The SST-related changes were higher in the south Atlantic part of the Southern Ocean, accounting for 30 % of changes in the total primary production. To explain the remaining variability in biological productivity, the authors also considered changes in atmospheric dust deposition. However, in this region, atmospheric dust supply tends to remain low, originating from small dust sources in Argentina, Australia and South Africa (Prospero et al. 2002) and a weak positive correlation between dust deposition and chlorophyll was found only in the west Pacific region of the Southern Ocean (Le Quéré et al. 2002). Their study demonstrates that simple assumptions about light limitation and nutrient (nitrogen and iron) limitation may not be sufficient to explain fully the observed variations in chlorophyll distribution.

**3.3.3.2 Continental Shelves and Coastal Regions** In continental shelves and coastal regions, additional physical processes may also control the supply of nutrient in the euphotic zone, including coastal upwelling, Ekman pumping and river outflow. In the eastern subtropical North Atlantic, between 10°N and 25°N, the negative correlation found between chlorophyll and SSH has been shown to result from an inverse relationship between SSH and nutricline depth (Pastor et al. 2014). In this region, the changes in nutricline depth and nutrient supply to the surface are governed primarily by changes in Ekman pumping (driving vertical advection processes), rather than by changes in stratification.

Atmospheric dust supply from the North African and Asian deserts, as well as coastal river discharge can also provide significant sources of nutrient supply for phytoplankton growth and modify the general latitudinal relationships between chlorophyll and SSH and between chlorophyll and SST. For instance, in the vicinity of the Amazon and Orinoco River plumes, positive relationships between chlorophyll and SST and chlorophyll and SSH are observed (Fig. 12a, b). The chlorophyll concentration and the concentration of coloured dissolved organic matter are higher in these river plumes than in surrounding waters (Smith and Demaster 1996; Hu et al. 2004). The location and direction of these river plumes are influenced by anticyclonic eddies, characteristic of higher SST and SSH, which are capable of transporting the plumes hundreds of miles offshore (Johns et al. 1990; Corredor et al. 2004).

**3.3.3.3 Effect of Eddies** A prominent feature is shown off Western Australia where there is a clear positive relationship between chlorophyll and SSH (Fig. 12a, c). In this region, anticyclonic eddies are thought to entrain shelf waters with regionally high chlorophyll concentration (Pearce and Griffiths 1991; Moore et al. 2007). These anticyclonic eddies then propagate westward and higher chlorophyll values are maintained through sub-mesoscale injection of nutrients into the anticyclonic-eddy boundary (Moore et al. 2007).

### **3.4 Bio-Optical Heating Influence on SST, Mixed Layer Depth (MLD), Air-Sea Flux and How it May Affect SSH**

The absorption of solar irradiance by phytoplankton cells (described in Sect. 2.3) has been shown to influence considerably the heating rate of the upper layer of the world oceans. Using a mixed layer model that incorporates ocean colour observations, Sathyendranath et al. (1991) examined the effect of light attenuation on surface temperature by comparing model results forced by a pure-water case, and by a chlorophyll-dependent case. The authors estimated biologically induced heating of surface temperature could reach a maximum of up to +4 °C from August to September in the Arabian Sea, using satellite data for 1979. Subsequently, several investigators have used three-dimensional ocean models to study the influence of phytoplankton on SST and MLD at the regional and global scales (e.g., Nakamoto et al. 2000; Manizza et al. 2005; Wu et al. 2007; Zhai et al. 2011). As phytoplankton absorb a significant fraction of the incident solar radiation and increase the temperature in the surface layer, less radiation penetrates to greater depths. The increased temperature contrast between surface and deep waters can enhance water column stability and reduce the depth of the mixed layer. For instance, Nakamoto et al. (2000) reported, in the Arabian Sea, a bio-optical heating of SST up to +0.6 °C and mixed layer depth decrease by 20 m. During the Summer season, in the Labrador Sea, Wu et al. (2007) showed SST changes between -1.0 and +2.0 °C, and mean MLD difference of 10 m (i.e. ~20–50 % shallower than it would be if phytoplankton were absent). Using a global ocean model, Manizza et al. (2005) observed temperature differences caused by the absorption of heat by phytoplankton between -0.2 and +0.6 °C at mid and high latitudes, with minimum values in winter and maximum values during the spring bloom. In their model results, the amplitude of the seasonal changes in the water column thermal structure and the MLD increased from low to high latitudes, with maximum MLD decrease by up to 20 m observed at 60° in both hemispheres.

Solar radiation and phytoplankton are not the only factor controlling SST and MLD in the oceans. Additional physical processes such as air-sea heat exchange, wind mixing and horizontal advection play important roles (see Sect. 3.2). Zhai et al. (2011) demonstrated increased heat loss from the ocean to the air associated with bio-optical heating of the upper ocean caused by the presence of phytoplankton in the Gulf of St. Lawrence. Atmospheric heat gain induced by the presence of phytoplankton has been further examined in coupled ocean-atmosphere models, which show an amplification of the seasonal cycle of temperature in the troposphere, modulating the tropical convection patterns and atmospheric circulation (Shell et al. 2003) and affecting large patterns of climate variability such as ENSO (Zhang 2015).

The strong influence of the absorption of solar irradiance by phytoplankton cells on the heating rate of the upper layer of the world oceans suggests that bio-optical heating should have an influence not only on SST but also on SSH. This hypothesis is further supported by the fact that SST and buoyancy-forced SSH show large common variability, which is due to the surface heat forcing (see Sect. 3.2.3).

## 4 Conclusions

In this paper, we have analysed the regional variability of observed SSH, SST and OC from the CCI datasets over the period 1993–2011. We have focused our analysis on the signature of the ocean large-scale climate fluctuations driven by the atmospheric forcing, and we did not consider the mesoscale activity, which has been filtered out. We used the ECCO version 4 ocean reanalysis to unravel the role of ocean transport and surface buoyancy fluxes in the ocean climate fluctuations and analyse the associated signatures on the observed SSH, SST and OC. Our analyses corroborate the findings from past studies on the role of ocean transport and surface buoyancy fluxes in the SSH variations at interannual to decadal timescales (Piecuch and Ponte 2011; Piecuch et al. 2013; Fukumori and Wang 2013; Forget and Ponte 2015). They also provide new insights on the role of ocean transport and surface buoyancy fluxes in the SST variations and on the relation between the SSH, SST and OC variations at interannual to decadal timescales.

In agreement with previous studies, we show that the variability and trends in observed SSH over the last two decades are largely dominated by the steric effect except in shallow shelf seas where the mass effect is of the same order of magnitude as the steric effect and at high latitudes ( $>60^{\circ}\text{N}$  and  $<55^{\circ}\text{S}$ ) where it dominates over the steric effect. The steric sea level signal is essentially due to temperature changes. Salinity changes play only a local role, but this role can be sizeable in several regions, in particular in the North Atlantic, in the Arctic and in the Southern Ocean. The ECCO reanalysis reveals that the observed steric sea level variability and trends are essentially forced by surface wind stress anomalies, in particular in the tropics where the SSH variability and trends are the most intense over the last two decades. The buoyancy forcing plays also a sizeable role but of smaller amplitude and more uniformly distributed. In the extra tropics, where the wind stress forcing effect on SSH is smaller, the buoyancy forcing effect becomes significant and explains a sizeable part of the SSH variability and trends. In general, on average over the ocean, the buoyancy forcing effect on SSH trends is positive which reflects the penetration of heat into the ocean and the global warming of the ocean (Gregory et al. 2001; Suzuki and Ishii 2011). This result confirms that different reasons explain the global sea level rise from ocean warming and the regional sea level rise. While the buoyancy fluxes only are responsible for the total heat that enters the ocean and the associated global mean sea level rise, both ocean transport divergences caused by wind stress anomalies and the non-uniform buoyancy forcing (essentially at mid to high latitudes) are responsible for the regional distribution of the heat within the ocean and thus for the regional sea level departures around the global mean.

Concerning the SST variability and trends over the last two decades, we show that the effect of local surface heat fluxes and ocean transport divergences locally is large and opposite to each other almost everywhere in the ocean. This finding primarily reflects the nature of the local steady-state SST budget (in our case, integrated over time), wherein local heat forcing is compensated for and entirely cancelled out by the action of ocean transport processes. However, the cancellation between local forcing and ocean transports is not exact, and the residual tendencies are what give rise to the resulting SST variability and trends. This result gives a unique perspective on the observed SST changes that, to our knowledge, has not been strongly emphasized elsewhere: almost everywhere, the mixed layer heat content is approximately in a local steady-state balance with the ocean transport divergences effect almost entirely compensating the heat fluxes effect; in this context, observed changes in SST are interpreted as relatively small departures from this

background steady-state. In terms of interannual variability in SST, the effect of the surface heat flux forcing is larger than the effect of the ocean transport almost everywhere except in the tropical Pacific where both play a similar role. In terms of trends in SST, the picture is not so clear: both effects play a dominant role but in different regions.

Thus, we have provided complementary descriptions of mechanisms responsible for SSH and SST variability and trends. On the one hand, our exploration of SSH was more dynamical, focusing on the relevant forcing mechanisms (namely winds or buoyancy), without pinpointing particular processes (e.g., circulation versus mixing). On the other hand, our investigation of SST was more kinematical, targeting the underlying physical processes (e.g., advection or diffusion), without identifying the responsible drivers in all cases (i.e. wind or buoyancy). These separate analyses put on display the capabilities of the ocean reanalysis machinery, and how such frameworks can help us understand, in a very detailed fashion, the nature of oceanic variability and change. In any case, bringing together the results of our SSH and SST analyses, we can see that SSH and SST bear some common variability. The main reason is that both SSH and SST variability show significant contributions from the surface heat fluxes forcing. This is evidenced by the high correlation between SST and buoyancy-forced SSH almost everywhere except in a few regions where the freshwater effect on buoyancy-forced SSH is dominant over the heat flux effect, as in the Pacific warm pool or in the Arctic region. In the tropics and in the upwelling regions, the wind stress forcing is also a cause of sizeable common variability in SST and SSH along with the surface heat flux forcing because wind stress variability in the tropics generate at the same time a zonal pressure gradient and a zonal tilt in the thermocline, which make, respectively, sea level and SST vary in phase in this region. SSH and SST bear also some common features in their trend patterns over the last two decades. However, the picture is more complicated than for the interannual to decadal variability. This indicates that probably the relationship between SST and buoyancy-forced sea level or wind forced sea level is quite complex in general, and likely depends critically on time-scale, among other factors.

OC is a variable that is fundamentally different from SST and SSH because it depends on biological processes, which are forced by underlying physical processes. The concentration of chlorophyll, the main photosynthetic pigment present in all phytoplankton cells, can be used as key measure of the phytoplankton population and is a central variable in models used to estimate primary production (the rate at which phytoplankton produces organic matter from dissolved inorganic CO<sub>2</sub>), and export production (approximately 20 % of net photosynthesis at global scale is exported to the deep ocean, indicating a strong coupling between biological activity and the oceanic carbon sink, Laws et al. 2000). The growth of phytoplankton is primarily governed by the availability of light and nutrients, which in turn depend mostly on climate forcing conditions. Thus, OC variability and trends bear a strong dependence on climate fluctuations, with implications for the oceanic primary production and export production, and can show significant correlations with SSH and SST. Although the correlation between OC and SSH tends to be weaker than between OC and SST, they display similar regional patterns throughout most of the global oceans. The tropics and subtropics show negative correlations because in these regions phytoplankton growth and export production are driven by nutrient availability in the mixed layer. Here, increases in nutrient availability are mainly driven by vertical entrainment (deeper mixed layers) and upwelling which influence SST (cooler waters entrained into the mixed layer) and SSH (surface divergence). At high latitudes, phytoplankton growth and export production are primarily driven by light availability. At these latitudes, changes in light at the sea surface are accompanied by warming of the waters which causes an increase in SST

and buoyancy-forced sea level and explain the positive correlation between OC, SSH and SST.

As discussed earlier, phytoplankton can have a feedback effect on climate fluctuations. The absorption of solar irradiance by phytoplankton pigments tends to increase the heating rate of surface layers, stabilize the water column and reduce the depth of the mixed layer. As a result it changes the distribution of the heat and the stratification in the upper ocean. Furthermore, it has been suggested that temperature might affect primary production and remineralization differently, and hence modulate biologically mediated air-sea carbon exchange (Matsumoto 2007). The regional effect of bio-optical feedbacks on SST has been reported by several studies as noted in Sect. 3.4, but no apparent effects on SSH have been reported yet. Given the significant influence of the absorption of solar irradiance by phytoplankton on the heating rate of the upper layer, and the importance of the surface heat fluxes in the SSH variability, we may speculate that bio-optical heating could influence SSH variability indirectly. However, it is not a trivial task to evaluate the influence of bio-optical heating on SSH and, to our knowledge, it has not been undertaken yet. Noting that localization of solar heating close to the surface would alter air-sea exchange of heat, a possible starting point for future studies could be to examine the impact of phytoplankton on the total heat content of the water column, which would impact SSH. The question remains whether such an impact could be a significant one.

**Acknowledgments** This work was supported by the CNES. It is based on observations from Topex/Poseidon, Jason 1/2, ENVISAT, ERS1/2 and Altikaa. The authors want to thank Gaël Forget (Massachusetts Institute of Technology) for providing the output of the ECCO perturbation forcing experiments and Ou Wang (Jet Propulsion Laboratory) for providing the fields necessary for computing the SST budgets. C.G. Piecuch participation was supported by NASA grant NNX14AJ51G. This paper is an outcome of the ISSI Workshop “Integrative Study of Sea Level Budget”, held in Bern in February 2015. M-F.R., S.S., and R.J.W.B. would like to acknowledge funding from the ESA Living Planet Fellowship programme, the ESA OC-CCI project and the NERC’s UK National Centre for Earth Observation.

## References

- Ablain M, Cazenave A, Larnicol G, Balmaseda M, Cipollini P, Faugère Y, Fernandes MJ, Henry O, Johannessen JA, Knudsen P, Andersen O, Legeais J, Meyssignac B, Picot N, Roca M, Rudenko S, Scharffenberg MG, Stammer D, Timms G, Benveniste J (2015) Improved sea level record over the satellite altimetry era (1993–2010) from the Climate Change Initiative project. *Ocean Sci* 11:67–82. doi:[10.5194/os-11-67-2015](https://doi.org/10.5194/os-11-67-2015)
- Abraham JP, Baringer M, Bindoff NL, Boyer T, Cheng LJ, Church JA, Conroy JL, Domingues CM, Fasullo JT, Gilson J, Goni G, Good SA, Gorman JM, Gouretski V, Ishii M, Johnson GC, Kizu S, Lyman JM, Macdonald AM, Minkowycz WJ, Moffitt SE, Palmer MD, Piola AR, Reseghetti F, Schuckmann K, Trenberth KE, Velicogna I, Willis JK (2013) A review of global ocean temperature observations: implications for ocean heat content estimates and climate change. *Rev Geophys* 51:450–483. doi:[10.1002/rog.20022](https://doi.org/10.1002/rog.20022)
- Boyd PW, Jickells T, Law CS, Blain S, Boyle EA, Buesseler KO, Coale KH, Cullen JJ, de Baar HJW, Follows M, Harvey M, Lancelot C, Levasseur M, Owens NPJ, Pollard R, Rivkin RB, Sarmiento J, Schoemann V, Smetacek V, Takeda S, Tsuda A, Turner S, Watson AJ (2007) Mesoscale iron enrichment experiments 1993–2005: synthesis and future directions. *Science* 315:612–617. doi:[10.1126/science.1131669](https://doi.org/10.1126/science.1131669)
- Brewin RJW, Hirata T, Hardman-Mountford NJ, Lavender SJ, Sathyendranath S, Barlow R (2012) The Influence of the Indian Ocean Dipole on interannual variations in phytoplankton size structure as revealed by earth observation. *Deep Sea Res II* 77–80:117–127. doi:[10.1016/j.dsr2.2012.04.009](https://doi.org/10.1016/j.dsr2.2012.04.009)
- Brewin RJW, Mélin F, Sathyendranath S, Steinmetz F, Chuprin A, Grant M (2014) On the temporal consistency of chlorophyll products derived from three ocean-colour sensors. *ISPRS J Photogramm Remote Sens* 97:171–184. doi:[10.1016/j.isprsjprs.2014.08.013](https://doi.org/10.1016/j.isprsjprs.2014.08.013)

- Buckley MW, Ponte RM, Forget G, Heimbach P (2014) Low-frequency SST and upper-ocean heat content variability in the North Atlantic. *J Clim* 27:4996–5018. doi:[10.1175/JCLI-D-13-00316.1](https://doi.org/10.1175/JCLI-D-13-00316.1)
- Cabanes C, Huck T, Colin de Verdière A (2006) Contributions of wind forcing and surface heating to interannual sea level variations in the Atlantic Ocean. *J Phys Oceanogr* 36(9):1739–1750
- Cayan DR (1992) Latent and sensible heat flux anomalies over the northern oceans: driving the sea surface temperature. *J Phys Oceanogr* 22:859–881
- Church JA, Clark PU, Cazenave A, Gregory JM, Jevrejeva S, Levermann L, Merrifield MA, Milne GA, Nerem RS, Nunn PD, Payne AJ, Pfeffer WT, Stammer D, Unnikrishnan AS (2013) Sea level change. In: Stocker TF, Qin D, Plattner GK, Tignor M, Allen SK, Boschung J, Nauels A, Xia Y, Bex V, Midgley PM (eds) *Climate change 2013: the physical science basis. Contribution of Working Group I to the fifth assessment report of the Intergovernmental Panel on Climate Change*. Cambridge University Press, Cambridge
- Corredor JE, Morell JM, Lopez JM, Capella JE, Armstrong RA (2004) Cyclonic eddy entrains Orinoco River Plume in eastern Caribbean. *EOS Trans Am Geophys Union* 85(20):197–202
- Dee D, Uppala S, Simmons A, Berrisford P, Poli P, Kobayashi S, Andrae U, Balmaseda M, Balsamo G, Bauer P, Bechtold P, Beljaars ACM, van de Berg L, Bidlot J, Bormann N, Delsol C, Dragani R, Fuentes M, Geer AJ, Haimberger L, Healy SB, Hersbach H, Hólm EV, Isaksen L, Kållberg P, Köhler M, Matricardi M, McNally AP, Monge-Sanz BM, Morcrette J-J, Park B-K, Peubey C, de Rosnay P, Tavolato C, Thépaut J-N, Vitart F (2011) The ERA-interim reanalysis: configuration and performance of the data assimilation system. *Q J R Meteorol Soc* 137(656):553–597. doi:[10.1002/qj.828](https://doi.org/10.1002/qj.828)
- Deser C, Alexander MA, Timlin MS (2003) Understanding the persistence of sea surface temperature anomalies in midlatitudes. *J. Clim* 16:57–72. doi:[10.1175/1520-0442\(2003\)016<0057:UTPOSS>2.0.CO;2](https://doi.org/10.1175/1520-0442(2003)016<0057:UTPOSS>2.0.CO;2)
- Deser C, Alexander MA, Xie SP, Phillips AS (2010) Sea surface temperature variability: patterns and mechanisms. *Ann Rev Mar Sci* 2:115–143. doi:[10.1146/annurev-marine-120408-151453](https://doi.org/10.1146/annurev-marine-120408-151453)
- Durack PJ, Wijffels SE, Gleckler PJ (2014) Long-term sea-level change revisited: the role of salinity. *Environ Res Lett* 9:114017. doi:[10.1088/1748-9326/9/11/114017](https://doi.org/10.1088/1748-9326/9/11/114017)
- Edwards AM, Platt T, Wright DG (2001) Biologically induced circulation at fronts. *J Geophys Res* 106:7081–7095. doi:[10.1029/2000JC000332](https://doi.org/10.1029/2000JC000332)
- Forget G, Ponte RM (2015) The partition of regional sea level variability. *Prog Oceanogr* 137:173–195. doi:[10.1016/j.pocean.2015.06.002](https://doi.org/10.1016/j.pocean.2015.06.002)
- Forget G, Campin JM, Heimbach P, Hill CN, Ponte RM, Wunsch C (2015) ECCO version 4: an integrated framework for non-linear inverse modeling and global ocean state estimation. *Geosci Model Dev* 8:3071–3104. doi:[10.5194/gmd-8-3071-2015](https://doi.org/10.5194/gmd-8-3071-2015)
- Frankcombe LM, Spence P, Hogg AM, England MH, Griffies SM (2013) Sea level changes forced by Southern Ocean winds. *Geophys Res Lett* 40:5710–5715. doi:[10.1002/2013GL058104](https://doi.org/10.1002/2013GL058104)
- Frankignoul C, Hasselmann K (1977) Stochastic climate models. Part 2. Application to sea-surface temperature variability and thermocline variability. *Tellus* 29:284–305. doi:[10.1111/j.2153-3490.1977.tb00740.x](https://doi.org/10.1111/j.2153-3490.1977.tb00740.x)
- Fu G, Baith KS, McClain CR (1998) The SeaWiFS data analysis system. In: *Proceedings of the 4th Pacific Ocean remote sensing conference, Qingdao, July 1998*, pp 73–79
- Fukumori I, Wang O (2013) Origins of heat and freshwater anomalies underlying regional decadal sea level trends. *Geophys Res Lett* 40:563–567. doi:[10.1002/grl.50164](https://doi.org/10.1002/grl.50164)
- Fukumori I, Wang O, Llovel W, Fenty I, Forget G (2015) A near-uniform fluctuation of ocean bottom pressure and sea level across the deep ocean basins of the Arctic Ocean and the Nordic Seas. *Prog Oceanogr* 134:152–172. doi:[10.1016/j.pocean.2015.01.013](https://doi.org/10.1016/j.pocean.2015.01.013)
- Gill A, Niller P (1973) The theory of the seasonal variability in the ocean. *Deep Sea Res* 20(2):141–177. doi:[10.1016/0011-7471\(73\)90049-1](https://doi.org/10.1016/0011-7471(73)90049-1)
- Gregory JM, Church JA, Boer GJ, Dixon KW, Flato GM, Jackett DR, Lowe JA, O'Farrell SP, Roeckner E, Russell GL, Stouffer RJ, Winton M (2001) Comparison of results from several AOGCMs for global and regional sea-level change 1900–2100. *Clim Dyn* 18:225–240. doi:[10.1007/s003820100180](https://doi.org/10.1007/s003820100180)
- Grodsky SA, Carton JA, Liu H (2008) Comparison of bulk sea surface and mixed layer temperatures. *J Geophys Res* 113:C10026. doi:[10.1029/2008JC004871](https://doi.org/10.1029/2008JC004871)
- Hu C, Montgomery ET, Schmitt RW, Muller-Karger FE (2004) The dispersal of the Amazon and Orinoco River water in the tropical Atlantic and Caribbean Sea: observation from space and S-PALACE floats. *Deep Sea Res II* 51:1151–1171. doi:[10.1016/j.dsr2.2004.04.001](https://doi.org/10.1016/j.dsr2.2004.04.001)
- Ishii M, Kimoto M (2009) Reevaluation of historical ocean heat content variations with time-varying XBT and MBT depth bias corrections. *J Oceanogr* 65:287–299. doi:[10.1007/s10872-009-0027-7](https://doi.org/10.1007/s10872-009-0027-7)
- Johns WE, Lee TN, Schott F, Zantopp RJ, Evans RH (1990) The North Brazil Current retroflection: seasonal structure and eddy variability. *J Geophys Res* 95:22103–22120. doi:[10.1029/JC095iC12p22103](https://doi.org/10.1029/JC095iC12p22103)

- Kahru M, Gille ST, Murtugudde R, Strutton PG, Manzano-Sarabia M, Wang H, Mitchell BG (2010) Global correlations between winds and ocean chlorophyll. *J Geophys Res*. doi:[10.1029/2010JC006500](https://doi.org/10.1029/2010JC006500)
- Kirk JTO (1994) *Light and photosynthesis in aquatic ecosystems*, 2nd edn. Cambridge University Press, New York
- Köhl A (2014) Detecting processes contributing to interannual halosteric and thermosteric sea level variability. *J Clim* 27:2417–2426. doi:[10.1175/JCLI-D-13-00412.1](https://doi.org/10.1175/JCLI-D-13-00412.1)
- Laws EA, Falkowski PG, Smith WOS Jr, Ducklow H, McCarthy JJ (2000) Temperature effects on export production in the open ocean. *Global Biogeochem Cycles* 14:1231–1246
- Le Quéré C, Bopp L, Tegen I (2002) Antarctic circumpolar wave impact on marine biology: a natural laboratory for climate change study. *Geophys Res Lett*. doi:[10.1029/2001GL014585](https://doi.org/10.1029/2001GL014585)
- Lewis MR, Cullen JJ, Platt T (1983) Phytoplankton and thermal structure in the upper ocean: consequences of nonuniformity in chlorophyll profile. *J Geophys Res* 88:2565–2570. doi:[10.1029/JC088iC04p02565](https://doi.org/10.1029/JC088iC04p02565)
- Llovel W, Lee T (2015) Importance and origin of halosteric contribution to sea level change in the southeast Indian Ocean during 2005–2013. *Geophys Res Lett* 42:1148–1157. doi:[10.1002/2014GL026211](https://doi.org/10.1002/2014GL026211)
- Makowski JK, Chambers DP, Bonin JA (2015) Using ocean bottom pressure from the gravity recovery and climate experiment (GRACE) to estimate transport variability in the southern Indian Ocean. *J Geophys Res Oceans* 120:4245–4259. doi:[10.1002/2014JC010575](https://doi.org/10.1002/2014JC010575)
- Manizza M, Le Quere C, Watson AJ, Buitenhuis ET (2005) Bio-optical feedbacks among phytoplankton, upper ocean physics and sea-ice in a global model. *Geophys Res Lett*. doi:[10.1029/2004GL020778](https://doi.org/10.1029/2004GL020778)
- Marshall J, Johnson H, Goodman J (2001) A study of the interaction of the North Atlantic Oscillation with ocean circulation. *J Clim* 14:1399–1421. doi:[10.1175/1520-0442\(2001\)014<1399:ASOTIO>2.0.CO;2](https://doi.org/10.1175/1520-0442(2001)014<1399:ASOTIO>2.0.CO;2)
- Matsumoto K (2007) Biology-mediated temperature control on atmospheric pCO<sub>2</sub> and ocean biogeochemistry. *Geophys Res Lett*. doi:[10.1029/2007GL031301](https://doi.org/10.1029/2007GL031301)
- McGregor S, Gupta AS, England MH (2012) Constraining wind stress products with sea surface height observations and implications for Pacific ocean sea level trend attribution. *J Clim* 25(23):8164–8176. doi:[10.1175/JCLI-D-12-00105.1](https://doi.org/10.1175/JCLI-D-12-00105.1)
- Meehl GA, Hu A, Arblaster JM, Fasullo J, Trenberth KE (2013) Externally forced and internally generated decadal climate variability associated with the Interdecadal Pacific Oscillation. *J Clim* 26:7298–7310. doi:[10.1175/JCLI-D-12-00548.1](https://doi.org/10.1175/JCLI-D-12-00548.1)
- Merchant CJ, Embury O, Roberts-Jones J, Fiedler E, Bulgin CE, Corlett GK, Good S, McLaren A, Rayner N, Morak-Bozzo S, Donlon C (2014) Sea surface temperature datasets for climate applications from phase 1 of the European Space Agency Climate Change Initiative (SST CCI). *Geosci Data J* 1:179–191. doi:[10.1002/gdj3.20](https://doi.org/10.1002/gdj3.20)
- Merrifield MA (2011) A shift in western tropical Pacific sea level trends during the 1990s. *J Clim* 24:4126–4138. doi:[10.1175/2011JCLI3932.1](https://doi.org/10.1175/2011JCLI3932.1)
- Meyssignac B, Salas y Melia D, Becker M, Llovel W, Cazenave A (2012) Tropical Pacific spatial trend patterns in observed sea level: internal variability and/or anthropogenic signature? *Clim Past* 8:787–802. doi:[10.5194/cp-8-787-2012](https://doi.org/10.5194/cp-8-787-2012)
- Moon JH, Song YT (2013) Sea level and heat content changes in the western North Pacific. *J Geophys Res Oceans* 118:2014–2022. doi:[10.1002/jgrc.20096](https://doi.org/10.1002/jgrc.20096)
- Moore TS, Matear RJ, Marra J, Clementson L (2007) Phytoplankton variability off the Western Australian Coast: mesoscale eddies and their role in cross-shelf exchange. *Deep Sea Res II* 54:943–960. doi:[10.1016/j.dsr2.2007.02.006](https://doi.org/10.1016/j.dsr2.2007.02.006)
- Nakamoto S, Kumar SP, Oberhuber JM, Muneyama K, Frouin R (2000) Chlorophyll modulation of sea surface temperature in the Arabian Sea in a mixed-layer isopycnal general circulation model. *Geophys Res Lett* 27:747–750. doi:[10.1029/1999GL002371](https://doi.org/10.1029/1999GL002371)
- Palanisamy H, Cazenave A, Delcroix T, Meyssignac B (2015) Spatial trend patterns in the Pacific Ocean sea level during the altimetry era: the contribution of thermocline depth change and internal climate variability. *Ocean Dyn*. doi:[10.1007/s10236-014-0805-7](https://doi.org/10.1007/s10236-014-0805-7)
- Pastor MV, Palter JB, Pelegri JL, Dunne JP (2014) Physical drivers of interannual chlorophyll variability in the eastern subtropical North Atlantic. *J Geophys Res* 118:3871–3886. doi:[10.1002/jgrc.20254](https://doi.org/10.1002/jgrc.20254)
- Pearce AF, Griffiths RW (1991) The mesoscale structure of the Leeuwin current—a comparison of laboratory models and satellite imagery. *J Geophys Res* 96:16739–16757. doi:[10.1029/91JC01712](https://doi.org/10.1029/91JC01712)
- Penduff T, Juza M, Barnier B, Zika J, Dewar WK, Treguier AM, Molines JM, Audren N (2011) Sea level expression of intrinsic and forced ocean variabilities at interannual time scales. *J Clim* 24:5652–5670. doi:[10.1175/JCLI-D-11-00077.1](https://doi.org/10.1175/JCLI-D-11-00077.1)
- Peralta-Ferriz C, Morison JH, Wallace JM, Bonin JA, Zhang JL (2014) Arctic Ocean circulation patterns revealed by GRACE. *J Clim* 27:1445–1468. doi:[10.1175/JCLI-D-13-00013.1](https://doi.org/10.1175/JCLI-D-13-00013.1)
- Piecuch CG, Ponte RM (2011) Mechanisms of interannual steric sea level variability. *Geophys Res Lett*. doi:[10.1029/2011GL048440](https://doi.org/10.1029/2011GL048440)

- Piecuch CG, Ponte RM (2012) Importance of circulation changes to Atlantic heat storage rates on seasonal and interannual time scales. *J Clim* 25:350–362. doi:[10.1175/JCLI-D-11-00123.1](https://doi.org/10.1175/JCLI-D-11-00123.1)
- Piecuch CG, Ponte RM (2013) Buoyancy-driven interannual sea level changes in the tropical South Atlantic. *J Phys Oceanogr* 43:533–547. doi:[10.1175/JPO-D-12-093.1](https://doi.org/10.1175/JPO-D-12-093.1)
- Piecuch CG, Quinn KJ, Ponte RM (2013) Satellite-derived interannual ocean bottom pressure variability and its relation to sea level. *Geophys Res Lett* 40:3016–3110. doi:[10.1002/grl.50549](https://doi.org/10.1002/grl.50549)
- Piecuch CG, Fukumori I, Ponte RM, Wang O (2015) Vertical structure of ocean pressure variations with application to satellite-gravimetric observations. *J Atmos Ocean Tech* 32:603–613. doi:[10.1175/JTECH-D-14-00156.1](https://doi.org/10.1175/JTECH-D-14-00156.1)
- Ponte RM, Piecuch CG (2014) Interannual bottom pressure signals in the Australian-Antarctic and Bellingshausen basins. *J Phys Oceanogr* 44(5):1456–1465. doi:[10.1175/JPO-D-13-0223.1](https://doi.org/10.1175/JPO-D-13-0223.1)
- Prospero JM, Ginoux P, Torres O, Nicholson SE, Gill TE (2002) Environmental characterization of global sources of atmospheric soil dust identified with the Nimbus 7 total ozone mapping spectrometer (TOMS) absorbing aerosol product. *Rev Geophys* 40:1002. doi:[10.1029/2000RG000095](https://doi.org/10.1029/2000RG000095)
- Purkey SG, Johnson GC, Chambers DP (2014) Relative contributions of ocean mass and deep steric changes to sea level rise between 1993 and 2013. *J Geophys Res Oceans* 119:7509–7522. doi:[10.1002/2014jc010180](https://doi.org/10.1002/2014jc010180)
- Qiu B, Chen S (2012) Multidecadal sea level and gyre circulation variability in the northwestern tropical Pacific Ocean. *J Phys Oceanogr* 42:193–206. doi:[10.1175/JPO-D-11-061.1](https://doi.org/10.1175/JPO-D-11-061.1)
- Racault MF, Raitos DE, Berumen ML, Brewin RJW, Platt T, Sathyendranath S, Hoteit I (2015) Phytoplankton phenology indices in coral reef ecosystems: application to ocean-color observations in the Red Sea. *Remote Sens Environ* 160:222–234. doi:[10.1016/j.rse.2015.01.019](https://doi.org/10.1016/j.rse.2015.01.019)
- Rhein M, Rintoul SR, Aoki S, Campos E, Chambers D, Feely RA, Gulev S, Johnson GC, Josey SA, Kostianoy A, Mauritzen C, Roemmich D, Talley LD, Wang F (2013) Observations: ocean. In: Stocker TF, Qin D, Plattner GK, Tignor M, Allen SK, Boschung J, Nauels A, Xia Y, Bex V, Midgley PM (eds) *Climate change 2013: the physical science basis. Contribution of Working Group I to the fifth assessment report of the Intergovernmental Panel on Climate Change*. Cambridge University Press, Cambridge, pp 255–316. doi:[10.1017/CBO9781107415324.010](https://doi.org/10.1017/CBO9781107415324.010)
- Sathyendranath S, Krasemann H (2014) Climate assessment report: Ocean Colour Climate Change Initiative (OC-CCI)—phase one (ESA OC-CCI, <http://www.esa-oceancolour-cci.org/?q=documents>)
- Sathyendranath S, Gouveia AD, Shetye SR, Ravindran P, Platt T (1991) Biological control of surface temperature in the Arabian Sea. *Nature* 349:54–56. doi:[10.1038/349054a0](https://doi.org/10.1038/349054a0)
- Sathyendranath S, Brewin RJW, Brockmann C, Brotas V, Ciavatta S, Chuprin A, Couto AB, Doerffer R, Dowell M, Grant M, Groom S, Horseman A, Jackson T, Krasemann H, Lavender S, Martinez Vicente V, Mélin Moore TS, Müller D, Regner P, Roy S, Steinmetz F, Swinton J, Taberner M, Thompson A, Valente A, Zühlke M, Brandt VE, Feldman G, Franz B, Frouin R, Gould Jr. RW, Hooker S, Kahru M, Mitchell MG, Muller-Karger F, Sosik HM, Voss KJ, Werdell J, Platt T (2016) Creating an ocean-colour time series for use in climate studies: the experience of the Ocean-Colour Climate Change Initiative. *Remote Sens Environ*. Under review
- Sérazin G, Penduff T, Grégorio S, Barnier B, Molines JM, Terray L (2015) Intrinsic variability of sea level from global ocean simulations: spatiotemporal scales. *J Clim* 28:4279–4292. doi:[10.1175/JCLI-D-14-00554.1](https://doi.org/10.1175/JCLI-D-14-00554.1)
- Shell KM, Frouin R, Nakamoto S, Somerville RCJ (2003) Atmospheric response to solar radiation absorbed by phytoplankton. *J Geophys Res*. doi:[10.1029/2003JD003440](https://doi.org/10.1029/2003JD003440)
- Siegel DA, Behrenfeld MJ, Maritorena S, McClain CR, Antoine D, Bailey SW, Bontempi PS, Boss ES, Dierssen HM, Doney SC, Eplee RE Jr, Evans RH, Feldman GC, Fields E, Franz BA, Kuring NA, Mengelt C, Nelson NB, Patt FS, Robinson WD, Sarmiento JL, Swan CM, Werdell PJ, Westberry TK, Wilding JG, Yoder JA (2013) Regional to global assessments of phytoplankton dynamics from the SeaWiFS mission. *Remote Sens Environ* 135:77–91. doi:[10.1016/j.rse.2013.03.025](https://doi.org/10.1016/j.rse.2013.03.025)
- Smith WO, Demaster DJ (1996) Phytoplankton biomass and productivity in the Amazon River plume: correlation with seasonal river discharge. *Cont Shelf Res* 16:291–319. doi:[10.1016/0278-4343\(95\)00007-N](https://doi.org/10.1016/0278-4343(95)00007-N)
- Stammer D, Cazenave A, Ponte RM, Tamisiea ME (2013) Causes for contemporary regional sea level changes. *Ann Rev Mar Sci* 5:21–46. doi:[10.1146/annurev-marine-121211-172406](https://doi.org/10.1146/annurev-marine-121211-172406)
- Steinmetz F, Deschamps PY, Ramon D (2011) Atmospheric correction in presence of sun glint: application to MERIS. *Opt Express* 19:9783–9800. doi:[10.1364/OE.19.009783](https://doi.org/10.1364/OE.19.009783)
- Suzuki T, Ishii M (2011) Regional distribution of sea level changes resulting from enhanced greenhouse warming in the model for interdisciplinary research on climate version 3.2. *Geophys Res Lett* 38:L02601. doi:[10.1029/2010GL045693](https://doi.org/10.1029/2010GL045693)

- Tamisiea ME (2011) Ongoing glacial isostatic contributions to observations of sea level change. *Geophys J Int* 186:1036–1044. doi:[10.1111/j.1365-246X.2011.05116.x](https://doi.org/10.1111/j.1365-246X.2011.05116.x)
- Thompson LA, Ladd CA (2004) The response of the North Pacific Ocean to decadal variability in atmospheric forcing: wind versus buoyancy forcing. *J Phys Oceanogr* 34:1373–1386. doi:[10.1175/1520-0485\(2004\)034<1373:TROTNP>2.0.CO;2](https://doi.org/10.1175/1520-0485(2004)034<1373:TROTNP>2.0.CO;2)
- Timmermann A, McGregor S, Jin FF (2010) Wind effects on past and future regional Sea level trends in the Southern Indo-Pacific\*. *J Clim* 23(16):4429–4437
- Turk D, McPhaden MJ, Busalacchi AJ, Lewis MR (2001) Remotely Sensed biological production in the equatorial Pacific. *Science* 293:471–474. doi:[10.1126/science.1056449](https://doi.org/10.1126/science.1056449)
- Visbeck M, Chassignet EP, Curry RG, Delworth TL, Dickson RR, Krahnmann K (2003) The ocean's response to North Atlantic Oscillation variability. In: Hurrell JW, Kushnir Y, Ottersen G, Visbeck M (eds) *The North Atlantic Oscillation: climatic significance and environmental impact*. American Geophysical Union, Washington, DC. doi:[10.1029/134GM06](https://doi.org/10.1029/134GM06)
- Volkov DL (2014) Do the North Atlantic winds drive the nonseasonal variability of the Arctic Ocean sea level? *Geophys Res Lett* 41:2041–2047. doi:[10.1002/2013GL059065](https://doi.org/10.1002/2013GL059065)
- Volkov DL, Landerer FW (2013) Non-seasonal fluctuations of the Arctic Ocean mass observed by the GRACE satellites. *J Geophys Res Oceans* 118:6451–6460. doi:[10.1002/2013JC009341](https://doi.org/10.1002/2013JC009341)
- Wilson C, Coles VJ (2005) Global climatological relationships between satellite biological and physical observations and upper ocean properties. *J Geophys Res* 110:C10001. doi:[10.1029/2004JC002724](https://doi.org/10.1029/2004JC002724)
- Wu Y, Tang CCL, Sathyendranath S, Platt T (2007) The impact of bio-optical heating on the properties of the upper ocean: a sensitivity study using a 3-D circulation model for the Labrador Sea. *Deep Sea Res II* 54:2630–2642. doi:[10.1016/j.dsr2.2007.08.019](https://doi.org/10.1016/j.dsr2.2007.08.019)
- Wunsch C, Heimbach P (2007) Practical global oceanic state estimation. *Phys D* 230:197–208. doi:[10.1016/j.physd.2006.09.040](https://doi.org/10.1016/j.physd.2006.09.040)
- Wunsch C, Stammer D (1997) Atmospheric loading and the oceanic “inverted barometer” effect. *Rev Geophys* 35:79–107. doi:[10.1029/96RG03037](https://doi.org/10.1029/96RG03037)
- Wunsch C, Ponte RM, Heimbach P (2007) Decadal trends in sea level patterns: 1993–2004. *J Clim* 20:5889–5911. doi:[10.1175/2007JCLI1840.1](https://doi.org/10.1175/2007JCLI1840.1)
- Zaneveld JRV, Kitchen JC, Pak H (1981) The influence of optical water types on the heating rate of a constant depth mixed layer. *J Geophys Res* 86:6426–6428
- Zhai L, Tang CCL, Platt T, Sathyendranath S (2011) Ocean response to attenuation of visible light by phytoplankton in the Gulf of St. Lawrence. *J Mar Syst* 88:285–297. doi:[10.1016/j.jmarsys.2011.05.005](https://doi.org/10.1016/j.jmarsys.2011.05.005)
- Zhang RH (2015) An ocean-biology-induced negative feedback on ENSO as derived from a hybrid coupled model of the tropical Pacific. *J Geophys Res Oceans*. doi:[10.1002/2015JC011305](https://doi.org/10.1002/2015JC011305)